ResearchGate

See discussions, stats, and author profiles for this publication at: https://www.researchgate.net/publication/332595099

# Geochemical evidence for thin syn-collision crust and major crustal thickening between 45 and 32 Ma at the southern margin of Tibet

**Article** *in* Gondwana Research · April 2019

DOI: 10.1016/j.gr.2019.03.011

CITATIONS
6

READS
562

**7 authors**, including:

Donald J Depaolo
University of California, Berkeley
**422** PUBLICATIONS **28,012** CITATIONS
SEE PROFILE

Matthew Wielicki
University of Alabama
**23** PUBLICATIONS **138** CITATIONS
SEE PROFILE

Zhidan Zhao
China University of Geosciences (Beijing)
**298** PUBLICATIONS **10,997** CITATIONS
SEE PROFILE

Di-Cheng Zhu
China University of Geosciences (Beijing)
**202** PUBLICATIONS **7,482** CITATIONS
SEE PROFILE

**Some of the authors of this publication are also working on these related projects:**



The Investigation of Continent-Continent Collision Between Tauride and Arabian Platforms Using Apatite Fission Track Thermochronology View project



Extensional Tectonics in Basins and Ranges, USA and Western Anatolia, Turkey View project

All content following this page was uploaded by Matthew Wielicki on 23 July 2019.

The user has requested enhancement of the downloaded file.

Gondwana Research 73 (2019) 123–135

Contents lists available at ScienceDirect

Gondwana Research

journal homepage: www.elsevier.com/locate/gr

# Geochemical evidence for thin *syn*-collision crust and major crustal thickening between 45 and 32 Ma at the southern margin of Tibet

Donald J. DePaolo [a,*], T. Mark Harrison [b], Matthew Wielicki [c], Zhidan Zhao [d], Di-Cheng Zhu [d], Hongfei Zhang [d], Xuanxue Mo [d]

[a] Department of Earth and Planetary Sciences, University of California, Berkeley, CA 94720, United States of America
[b] Department of Earth, Planetary and Space Sciences, University of California, Los Angeles, CA 90095, United States of America
[c] Department of Geological Sciences, University of Alabama, Tuscaloosa, AL 35487, United States of America
[d] School of Earth Science and Resources, China University of Geosciences, Beijing 100083, China

ARTICLE INFO

*Article history:*
Received 11 January 2018
Received in revised form 24 February 2019
Accepted 12 March 2019
Available online 23 April 2019

ABSTRACT

Geochemical data on widely distributed igneous rocks of southern Tibet are used to reconstruct paleo-crustal thickness during the 50+ million years that have elapsed since the onset of the India-Asia collision. We use two approaches, one based on Nd isotopes and an assimilation-recharge model for granitic magma genesis and another empirical method based on trace element geochemistry (La/Yb). The focus is on granitic rocks of two age ranges in a segment of the southern Lhasa Block between approximately 89.5° and 92.5°E longitude. One age range, 45 to 62 Ma, spans the time of the onset of collision and for which we infer the geochemistry of granitic rocks reflects mainly pre-collision structure. The other age range is 21 to 9 Ma for the Nd isotopic approach, and 32 to 9 Ma for La/Yb, where the geochemistry must reflect post-collision structure. Our results suggest that the pre- and *syn*-collision southern margin of the Lhasa block, that portion now located within 50–60 km of the Indus-Yarlung suture (IYS) and south of 29.8°N latitude was relatively thin, about 25–35 km thick until 45 Ma. At approximately 29.8°-29.9°N latitude there was a pronounced crustal discontinuity, and north of that latitude (for a distance that we cannot constrain), the inferred crustal thickness was greater, at least 50–55 km, as indicated by latest Cretaceous and Early Tertiary granitoids and ignimbrites that have large fractions of assimilated continental crust and high La/Yb ratios. Post-collision Nd isotopic and La/Yb data from granitoids younger than 32 Ma suggest that the southern margin south of 29.8°N was thickened substantially to at least 55–60 km (based on Nd isotopes) and possibly as much as 70–75 km (based on La/Yb) by Early to mid-Miocene time. These observations require that thickening of the southern Lhasa Block margin in the period 45–32 Ma was non-uniform; the crust now within 60 km of the suture was thickened by approximately 40 km whereas the crust north of 29.9°N latitude was thickened much less, or not at all. The region currently between 29.8°N and the YTS may have been the highest elevation mountain terrane in the period from roughly 30 to 20 Ma. The amount of Miocene denudation reflects this difference, as there is evidence of substantially more denudation near the IYS than in the region north of 29.9°N. Some of the difference in thickening could be due to magmatic additions from the mantle in the region south of 29.8°N, but there is need for at least 30 km of tectonic thickening between 45 and 32 Ma. The non-uniform thickening suggests that the high elevations at the southern margin of the Himalaya-Tibet orogen propagated southward by about 200 km, from north of Lhasa to their present position, during the period from 50 to 20 Ma. Present crustal thickness requires an additional 10–15 km of more uniform post-Miocene thickening.

© 2019 International Association for Gondwana Research. Published by Elsevier B.V. All rights reserved.

## 1. Introduction

Modern Tibet is the largest region of continental crust that is thicker than 60 km, and much of the plateau has crust thicker than 70 km (Pasyanos et al., 2014; Laske et al., 2012; Nabelek et al., 2009; Xu et al., 2013; Tenzer and Chen, 2014; Chen, 2017). Longstanding questions concern when the plateau reached its present elevation and crustal thickness, to what degree there are regional differences, and how that thickening history relates to the tectonics of the India-Asia collision (Bird, 1978; Copeland et al., 1987; Dewey et al., 1988; Molnar et al., 1993; Molnar, 2005; Yin and Harrison, 2000; Tapponnier et al., 2001; DeCelles et al., 2002; Clark et al., 2005; Currie et al., 2005; Dai et al., 2013; Ding et al., 2014; Wang et al., 2014). In this study we use the geochemistry of granitic rocks in central southern Tibet to investigate the timing and spatial variability of crustal thickening in the

* Corresponding author.
*E-mail address:* depaolo@eps.berkeley.edu (D.J. DePaolo).

https://doi.org/10.1016/j.gr.2019.03.011
1342-937X/© 2019 International Association for Gondwana Research. Published by Elsevier B.V. All rights reserved.

southernmost part of the Asian continent over the time period from 50 to 10 Ma. The geochemical methods involve the isotopes of Neodymium, an approach described in this work, and the concentrations of rare earth elements, in particular the La/Yb ratio approach (Chapman et al., 2015; Profeta et al., 2015; Farner and Lee, 2017; Hu et al., 2017). This study is an extension of recent work by Zhu et al. (2017), but employing also the Nd isotope approach and investigating spatial variability.

The southernmost structural province of Tibet, referred to as the Lhasa Block, is amenable to the geochemical approaches because it contains extensive Mesozoic to late-Cenozoic granitoid batholiths referred to as the Gangdese batholith (Xu et al., 1985; Harrison et al., 1992; Yin and Harrison, 2000; many others) (Fig. 1). The batholith is overlain in its northern part by widely distributed, mostly Eocene, ignimbrites of the Linzizong volcanic province (Allégre et al. 1984; Coulon et al. 1986; Leeder et al., 1988). The main volume of plutonic rocks was emplaced between the Late Cretaceous and Eocene, with a predominance of early Cenozoic ages (e.g. Zhu et al., 2017). The batholith is believed to represent continental margin magmatism associated with northward subduction of the Tethys oceanic crust under Asia prior to, and partly contemporaneous with, the India-Asia collision (Yin and Harrison, 2000). Based on a compilation of U—Pb ages, Zhu et al. (2017) propose that the peak in magmatic production was at 52–48 Ma, with the full width of the last large magmatic pulse being from about 60 to 40 Ma (see also Ji et al., 2011). The Indo-Asian collision is generally thought to have commenced by 56–58 Ma with large scale contact ("hard collision") occuring during the subsequent 10–15 Ma (Yin and Harrison, 2000; DeCelles et al., 2014; Hu et al., 2015). The large Gangdese magmatic pulse occurs slightly *after* the time of the onset of continent-continent collision, but coincident with the time at which the convergence velocity was decreasing markedly (Cande et al., 2010).

In this study, we present new isotopic data and review the available data on the Nd and Sr isotopic compositions and La/Yb ratios of the granitoid rocks emplaced in the region that is currently within about 150 km north of the Indus-Yarlung suture (IYS) in an east-west segment of the Gangdese batholith near Lhasa between about 89.5°E and 92.5°E longitude where there is relatively dense sampling. The objective is to evaluate systematic variations that could yield information on the evolution of crustal structure and its variability on a 10–100 km scale. Many

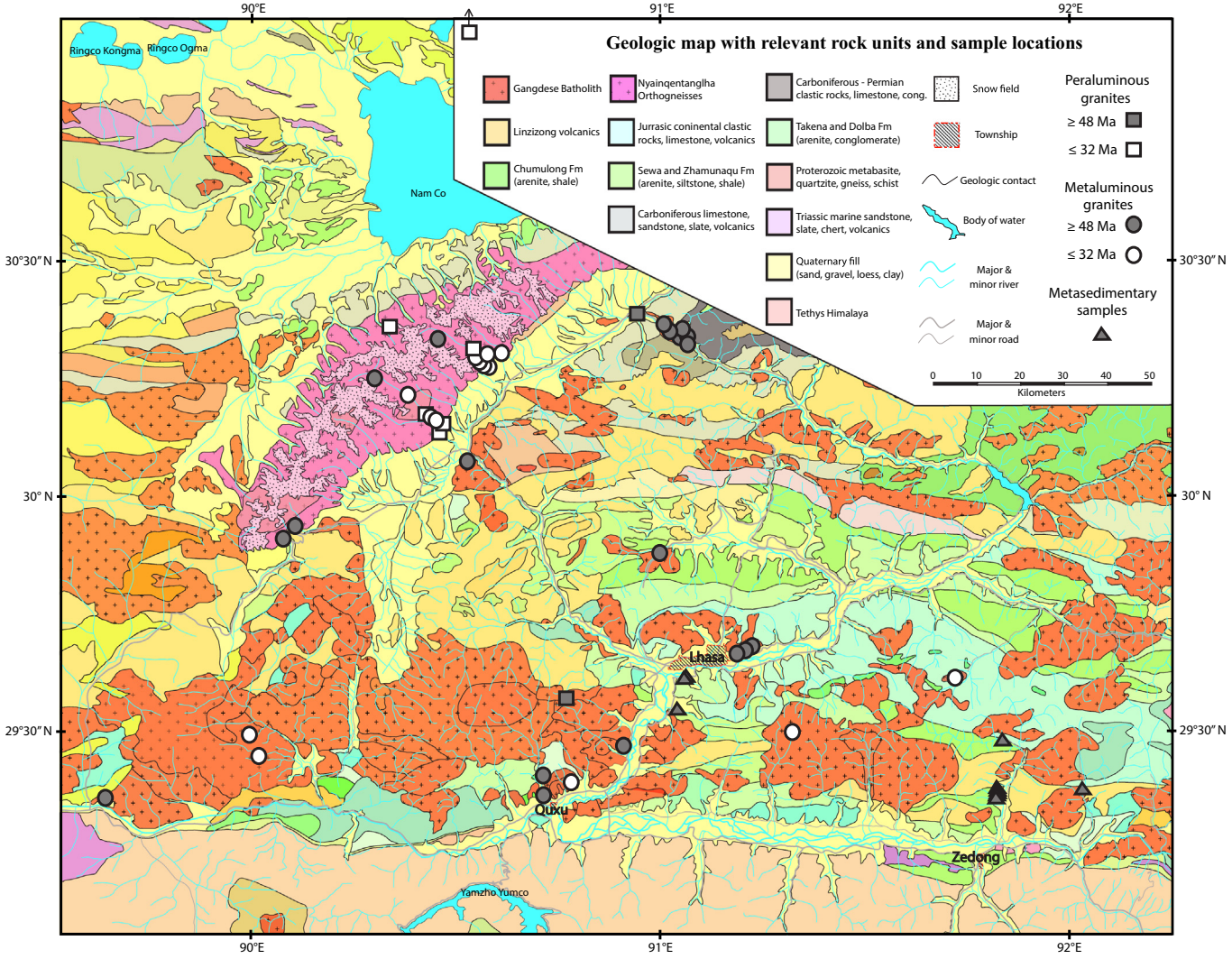


**Fig. 1.** Geologic map of portion of southeast Tibet covering ~50,000 km$^2$ from longitude 89.5 to 92.3 E and latitude 29 to 31 N, showing the distribution of calc-alkaline granitic (red-purple) and metasedimentary units (green) sampled in this study as well as other relevant geologic units (modified from 1:250,000 scale maps from China University of Geosciences Press Co., Ltd. including: Dangxiong District, H46C002001; Memba District, H46C002002; Lhasa District, H46C003001; Zedong District, H46C003002. Western portion, west of 90E, modified from Kidd et al., 1988. Further modification made from multiple field expeditions throughout the area by the authors and colleagues. Squares, circles and triangles indicate locations of samples (see table for references) used for Nd isotope analyses. Squares and circles show locations of peraluminous and metaluminous granites, respectively, and pre- or post-collisional crystallization age with grey fill indicating >48 Ma and white fill representing < 32 Ma. Grey triangles show locations of pre-collisional metasedimentary units sampled.

previous studies have reported isotopic data on granitoids from this region and more broadly across the batholith, and we use those results in this study (see Chapman et al., 2017; Zhu et al., 2015 for data compilations, and references in Tables). Most of the previous work has taken a broad view of the batholith and made conclusions about crustal structure based on the predominance of the data, although Chapman et al. (2017) and Zhu et al. (2015) also evaluate isotopic gradients on a 100 km scale.

The Nd isotopic and La/Yb data, for which we have the most coverage, exhibit systematic regional variations over the study area, and in general the compositions vary most strongly South-to-North, parallel to the direction of convergence. There are large Nd isotopic variations, about 15 units of $\varepsilon_{Nd}$, and large variations in normalized La/Yb (from 4 to 80). We discuss possible interpretations of the Nd isotopic pattern and argue that the isotopic variations largely reflect pre-batholithic crustal thickness variations, an interpretation that differs from that of Chapman et al. (2017). Although it is difficult to prove beyond doubt that crustal thickness is the primary variable affecting granitoid isotopic composition, we provide arguments why it is likely and an internally consistent interpretation of the data, provide algorithms for converting Nd isotopic composition to paleo-crustal thickness, and also show that the results from this approach are consistent with and potentially complementary to the La/Yb approach described by Profeta et al. (2015), Farner and Lee (2017), and Hu et al. (2017). This combined geochemical approach is potentially a broadly applicable means of obtaining paleo-crustal thickness information for convergent margins, and in the case of southern Tibet, suggests previously unrecognized aspects of the crustal thickening history.

## 2. Samples and analytical procedures

The Nd and Sr isotopic data used for this study include new measurements on 19 samples of intrusive rocks and 7 samples of metasedimentary rocks. The samples were collected by the authors in 2005–2014 or are samples reported on in Kapp et al. (2005), to some of which we have added new Nd isotopic analyses. We also include data from an additional 51 intrusive samples taken from the literature (Kapp et al., 2005; Mo et al., 2007; Gao et al., 2007; Hou et al., 2004, Nomade et al., 2004). The La/Yb data used are largely from the database of Chapman et al. (2017) with additional data from the samples we have collected and analyzed. The area of study is restricted to the region near Lhasa where there is relatively dense sample coverage, from about 89.5°E to 92.5°E longitude, and from the Yarlung-Tsangpo suture northward for approximately 150 km. The geologic map (Fig. 1) was compiled from multiple sources and in some areas modified by our field observations. It is an up-to-date representation of the geology of this area of some 30,000 km$^2$, with the geology referenced to a topographic base. The geochemical data used for the present work are summarized in Tables 1 and 2, and in Appendix B.

The Sr and Nd isotopic analyses (Tables 1 and 2) were done at the Center for Isotope Geochemistry at U.C. Berkeley using standard analytical procedures. Powdered samples were dissolved in a mixture of HF and $HClO_4$, then dried and redissolved in HCl. Sr and REE were separated on a first ion exchange column using HCl as elutriant. Nd was separated from other REE on a separate ion exchange column using 2-methylactic acid. Where they had not been previously determined by XRF or other means, concentrations of Rb, Sr, Sm and Nd were determined on separate aliquots of dissolved rock using a mixed spike technique with no chemistry; uncertainties are approximately ±3% on these concentration measurements. Sr and Nd isotopic compositions were measured on Thermo-Finnigan "Triton" TIMS instruments. The $^{87}Sr/^{86}Sr$ ratios are reported as raw measured values, corrected for mass discrimination using $^{84}Sr/^{86}Sr = 0.1194$. The standard SRM915 value for $^{87}Sr/^{86}Sr$ ratios is 0.71025 ± 2; very close to the accepted value. For Nd, the isotope ratios are measured using $Nd^+$ ions and a double filament technique and normalized to $^{146}Nd/^{144}Nd = 0.7219$, which makes the modern chondritic value of $^{143}Nd/^{144}Nd$ equal to 0.512636. Uncertainties on $^{87}Sr/^{86}Sr$ ratios are typically ±0.000015, and for $^{143}Nd/^{144}Nd$ ± 0.000010; both are negligible for this work and are not reported separately in the tables.

The $^{143}Nd/^{144}Nd$ ratios are also reported as $\varepsilon_{Nd}$ values, calculated according to:

$$\varepsilon_{Nd} = 10000\left[\frac{^{143}Nd/^{144}Nd_{sample}}{^{143}Nd/^{144}Nd_{chondrites}} - 1\right]$$

The $\varepsilon_{Nd}$ value can be defined at any time during the geologic evolution of the rock sample. For igneous rocks we define $\varepsilon_{Nd}(0)$ as the measured value relative to the modern chondritic value. At another time, $t$, such as the crystallization age of an igneous rock, the value $\varepsilon_{Nd}(t)$ is defined as the value the rock sample had at time "$t$" relative to the value of average chondrites at that time. The $^{143}Nd/^{144}Nd$ ratios for both sample and chondrites are calculated from the modern/measured values to account for radioactive decay of $^{147}Sm$ to $^{143}Nd$. For this calculation we use $\lambda_{Sm} = 6.54 \times 10^{-12}$ yr$^{-1}$, and a chondritic $^{147}Sm/^{144}Nd = 0.1954$. For our purposes, since the Nd isotopic variations are so large and they vary minimally on a 20–50 million year time scale, we have calculated all $\varepsilon_{Nd}(t)$ using an age of 50 Ma.

## 3. Isotopic composition of granitoids and pre-intrusive rocks

The Nd isotopic data from >45 Ma granitoids (Table 1) are plotted in Fig. 2 against latitude and against $^{87}Sr/^{86}Sr$. Latitude is a good indicator of distance north of the Indus-Yarlung suture, since the suture trends almost precisely east-west at this longitude. The latitude of the IYS is 29.25°N and the latitude of Lhasa is 29.67°N. Data are plotted separately for this main phase of Gangdese magmatism (pre-45 Ma; Fig. 2), which are pre-and *syn*-collisional, and the clearly post-collisional granites, which are all younger than 32 Ma (Fig. 3). The 45–62 Ma grouping represents the main pulse of Gangdese magmatism, so the voluminous intrusives provide sufficient areal sample coverage. We infer that the granitoid compositions in this group reflect mainly the magma generation conditions prior to major changes in the structure of the southern margin of Asia due to the collision. The 32 million year upper age limit for the younger group is somewhat arbitrary, but reflects the fact that there is a significant gap in ages between 45 and 32 Ma. Data from the pre-45 Ma samples are shown in Fig. 3 for comparison to the data from younger samples.

Nd isotopic data from the pre-45 Ma granites show a strong and systematic north-south gradient in $\varepsilon_{Nd}$, with mantle-like values (up to +5) adjacent to the suture (IYS) dropping to $\varepsilon_{Nd} \approx -10$ to −12 at 100 km north of the suture. We note that Zhu et al. (2011) also found north-south gradients in Hf isotopes measured in granitic *zircons* from samples both East and West of 90°E that are broadly consistent with the Nd isotopic results for whole rocks presented here. Chapman et al. (2017) also report a north-south trend in $\varepsilon_{Nd}$ and $\varepsilon_{Hf}$ (partly using the data also used here) although they did not restrict the longitudinal range, or age range, of their analysis and hence find somewhat less distinct trends.

The Nd isotopic data on granitoids need to be evaluated in the context of the isotopic composition of pre-batholithic crustal rocks that may have contributed to magma genesis. Although there are limited basement exposures (e.g., Amdo Gneiss; Harris et al., 1988), Cretaceous and Early Tertiary two-mica granites across the Lhasa terrane (e.g., Kapp et al., 2005; Mo et al., 2007; Tables 1 and 2) are likely to provide an indication of the $\varepsilon_{Nd}$ value of continental basement where they occur (Bennett and DePaolo, 1987). To further constrain the crustal $\varepsilon_{Nd}$ value that might characterize the crustal component for the pre-45 Ma granitoids we use new measurements of sub-greenschist metasedimentary rocks that occur in extensive exposures south and east of Lhasa (Table 3 and Fig. 1). Sedimentary rocks provide information on upper crustal rocks that were exposed at the time of their

**Table 1**
Location, isotopic and age data for granitic rocks older than ca. 45 Ma.
Data sources: This work; Kapp et al. (2005), Mo et al. (2007).

| Sample | Lithology | Latitude | Longitude | Location | Age (Ma) | $SiO_2$ | Sr | $^{87}Rb/^{86}Sr$ | $^{87}Sr/^{86}Sr$ | $^{87}Sr/^{86}Sr(50)$ | Nd | $^{147}Sm/^{144}Nd$ | $^{143}Nd/^{144}Nd$ | $\varepsilon_{Nd}(0)$ | $\varepsilon_{Nd}(50)$ | NCI[a] | $T_a$[b] | h (km)[b] | La/Yb(N) |
|---|---|---|---|---|---|---|---|---|---|---|---|---|---|---|---|---|---|---|---|
| RB1 | Granite | 29°21.348′ | 89°41.173′ | QR | 50 | 57.2 | 652 | 0.21 | 0.70407 | 0.70392 | 17.32 | 0.1312 | 0.512806 | 3.32 | 3.73 | 0.237 | 398 | 18.2 | 6.84 |
| RB4 | Granodiorite | 29°21.348′ | 89°41.173′ | QR | 50 | 66.4 | 410 | 0.86 | 0.70482 | 0.70420 | 9.10 | 0.1202 | 0.512803 | 3.26 | 3.74 | 0.237 | 397 | 18.2 | 17.14 |
| RB7 | Granite | 29°21.348′ | 89°41.173′ | QR | 50 | 76.0 | 186 | 1.32 | 0.70607 | 0.70513 | 15.52 | 0.0846 | 0.512757 | 2.36 | 3.07 | 0.274 | 434 | 20.6 | 17.01 |
| RB10 | Gabbro | 29°21.348′ | 89°41.173′ | QR | 50 | 50.8 | 895 | 0.02 | 0.70397 | 0.70396 | 19.53 | 0.1294 | 0.512719 | 1.62 | 2.04 | 0.331 | 488 | 24.3 | 5.33 |
| RB12 | Gabbro | 29°21.348′ | 89°41.173′ | QR | 50 | 54.7 | 910 | 0.08 | 0.70405 | 0.70399 | 17.30 | 0.1067 | 0.512724 | 1.72 | 2.29 | 0.317 | 475 | 23.5 | 11.22 |
| RB15 | Gabbro | 29°21.348′ | 89°41.173′ | QR | 50 | 49.8 | 812 | 0.21 | 0.70404 | 0.70389 | 19.89 | 0.1308 | 0.512771 | 2.63 | 3.04 | 0.275 | 436 | 20.7 | 7.51 |
| LS2 | Quartz monzonite | 29°53.227′ | 91°00.211′ | Q | 50 | 69.6 | 310 | 1.40 | 0.70616 | 0.70517 | 28.41 | 0.1191 | 0.512561 | −1.46 | −0.97 | 0.427 | 573 | 30.4 | 7.72 |
| LS3 | Diorite enclave | 29°53.227′ | 91°00.211′ | Q | 50 | 54.1 | 431 | 0.74 | 0.70556 | 0.70503 | 25.78 | 0.1451 | 0.512595 | −0.80 | −0.48 | 0.404 | 553 | 28.9 | 3.88 |
| LS4 | Diorite | 29°40.860′ | 91°15.586′ | Q | 50 | 54.2 | 528 | 0.18 | 0.70471 | 0.70458 | 16.34 | 0.1341 | 0.512722 | 1.68 | 2.07 | 0.282 | 442 | 21.2 | 3.95 |
| LS5 | Diorite | 29°40.398′ | 91°14.288′ | Q | 50 | 56.1 | 454 | 0.22 | 0.70492 | 0.70476 | 14.79 | 0.1404 | 0.512713 | 1.50 | 1.85 | 0.293 | 452 | 21.9 | 4.09 |
| LS7 | Granite | 29°40.084′ | 91°13.164′ | Q | 50 | 71.3 | 291 | 1.08 | 0.70552 | 0.70476 | 16.22 | 0.1157 | 0.512680 | 0.86 | 1.37 | 0.316 | 474 | 23.3 | 6.56 |
| 05DLB-03 | Gabbro | 29°24.13′ | 90°43.04′ | Q | 50 | 51.0 | 430 | 0.77 | 0.70391 | 0.70336 | 10.89 | 0.1417 | 0.512922 | 4.93 | 5.27 | 0.151 | 309 | 12.5 | |
| 05-DLB-04 | Tonalite | 29°21.97′ | 90°43.54′ | Q | 50 | 59.6 | 382 | 0.39 | 0.70450 | 0.70423 | 17.97 | 0.1208 | 0.512885 | 4.20 | 4.68 | 0.185 | 344 | 14.7 | |
| 05-DLB-06 | Granodiorite | 29°28.26′ | 90°55.9′ | QR | 50 | 64.5 | 331 | 0.49 | 0.70532 | 0.70497 | 26.18 | 0.2608 | 0.512679 | 0.18 | −0.24 | 0.458 | 598 | 32.3 | |
| 05-DLB-23 | Two-mica granite | 30°22.8′ | 90°55.83′ | Y | 200 | 73.5 | 31 | 49.22 | 0.79238 | | 10.40 | 0.1740 | 0.511981 | −13.44 | −12.90 | | | | |
| T-35 | Biotite granite | 30°04′ | 90°32′ | Y | 50 | 70.5 | 271 | | | | 32.13 | 0.1056 | 0.512386 | −4.88 | −4.30 | 0.615 | 715 | 41.2 | 10.30 |
| T-36 | Biotite granite | 30°04′ | 90°32′ | Y | 50 | 70.5 | 314 | | | | 35.86 | 0.1023 | 0.512484 | −2.97 | −2.37 | 0.519 | 646 | 35.8 | 11.87 |
| T-40 | Biotite granite | 30°04′ | 90°32′ | Y | 50 | 70.7 | 314 | | | | 32.82 | 0.1029 | 0.512419 | −4.23 | −3.64 | 0.582 | 692 | 39.4 | 10.12 |
| 99-7-26-1b | Two-mica granite | 29°35.0′ | 90°46.0′ | Ny | 213 | 76.5 | 45 | 25.45 | 0.77814 | | 10.90 | 0.1498 | 0.511962 | −13.15 | −11.91 | | | | |
| 99-5-2-1a | Granite | | | Ny | 54 | | | 5.67 | 0.71143 | 0.70708 | | 0.1028 | 0.512426 | −4.10 | −3.46 | 0.573 | 686 | 38.9 | |
| 99-5-5-4d | Granite | 29°54.0′ | 90°05.6 | Ny | 55 | 70.7 | 168 | 3.50 | 0.70906 | 0.70633 | 27.80 | 0.1066 | 0.512454 | −3.55 | −2.92 | 0.546 | 666 | 37.4 | 11.06 |
| 99-5-7-3b | Granite | 29°55.8′ | 90°08.3′ | Ny | 130 | 74.7 | 134 | 4.54 | 0.71164 | 0.70326 | 24.20 | 0.1019 | 0.512241 | −7.71 | −6.15 | | | | |
| 99-5-9-4a | Orthogneiss | 30°19.0′ | 90°27.5′ | Ny | 61 | 79.9 | 73 | 6.51 | 0.72415 | 0.71851 | 20.50 | 0.1253 | 0.512044 | −11.55 | −11.00 | 0.950 | 892 | 55.8 | |
| 99-5-11-1a | Biotite-granite | 30°15.0′ | 90°18.5′ | Ny | 88 | 68.9 | 517 | 1.97 | 0.70964 | 0.70718 | 29.50 | 0.0914 | 0.512344 | −5.70 | −4.53 | | | | 25.05 |
| 08DX04 | Granodiorite | 30°20.310′ | 91°04.105′ | Da | 54 | 64.5 | 460 | 1.53 | 0.71060 | 0.70942 | 53.40 | 0.1090 | 0.512269 | −7.20 | −6.60 | 0.730 | 787 | 46.9 | 14.09 |
| 08DX05 | Granodiorite | 30°20.442′ | 91°04.484′ | Da | 54 | 64.0 | 280 | 2.48 | 0.71104 | 0.70914 | 37.50 | 0.1048 | 0.512174 | −9.05 | −8.42 | 0.821 | 836 | 51.0 | 15.29 |
| 08DX06 | Granite | 30°20.442′ | 91°04.084′ | Da | 54 | 70.8 | 470 | 1.52 | 0.71057 | 0.70940 | 49.10 | 0.1143 | 0.512272 | −7.14 | −6.58 | 0.729 | 786 | 46.9 | 12.63 |
| 08DX08 | Gabbro | 30°20.779′ | 91°03.749′ | Da | 54 | 52.6 | 905 | 0.51 | 0.70818 | 0.70779 | 53.00 | 0.1233 | 0.512386 | −4.92 | −4.42 | 0.621 | 719 | 41.5 | 10.49 |
| 08DX11 | Gabbro | 30°20.916′ | 91°03.365′ | Da | 54 | 51.0 | 845 | 0.34 | 0.70850 | 0.70824 | 32.80 | 0.1237 | 0.512391 | −4.82 | −4.32 | 0.616 | 716 | 41.2 | 11.67 |
| 08DX14 | Granite | 30°21.226′ | 91°02.866′ | Da | 54 | 70.5 | 293 | 2.74 | 0.71153 | 0.70943 | 44.10 | 0.1084 | 0.512199 | −8.56 | −7.96 | 0.798 | 824 | 50.0 | 10.13 |

QR = Quxu-Renbo; Q = Quxu; Y = Yangbajing; Ny = Nyangentangla Range; Da = Damxung.
[a] NCI calculated using crustal $\varepsilon_{Nd}$ of −10 for Latitudes < 30°N and −12 for latitudes > 30°N; mantle $\varepsilon_{Nd}$ = +8.
[b] $T_a$ = assimilation temperature and h = crustal thickness; see Appendix.

**Table 2**
Location, isotopic and age data for granitic rocks younger than 32 Ma.
Data sources: This work; Kapp et al. (2005), Mo et al. (2007), Gao et al. (2007), Hou et al. (2004), Nomade et al. (2004).

| Sample | Lithology | | Location | Latitude | Longitude | Age (Ma) | $SiO_2$ | Sr (ppm) | $^{87}Rb/^{86}Sr$ | $^{87}Sr/^{86}Sr$ | $^{87}Sr/^{86}Sr$ (20) | Nd (ppm) | $^{147}Sm/^{144}Nd$ | $^{143}Nd/^{144}Nd$ | $\varepsilon_{Nd}$ (0) | $\varepsilon_{Nd}(t)$ | NCI[a] | $T_a$[b] | h (km)[b] | La/Yb (N) |
|---|---|---|---|---|---|---|---|---|---|---|---|---|---|---|---|---|---|---|---|---|
| 05-DLB-21 | Silicic tuff | This work | M | 29.76 | | 20 | | 276 | 1.541 | 0.70745 | 0.70701 | 34.87 | 0.1177 | 0.512322 | −6.11 | −5.92 | 0.994 | 908 | 57.2 | |
| T-42 | Two-mica granite | Zhidan | Y | 30°06′ | 90°32′ | 32 | 77.3 | 5 | | | | 14.26 | 0.2099 | 0.512240 | −7.72 | *−7.76* | *0.985* | *905* | *56.9* | |
| T-44 | Two-mica granite | Zhidan | Y | 30°07′ | 90°32′ | 32 | 77.1 | 5 | | | | 13.46 | 0.2287 | 0.512177 | −8.95 | *−9.04* | *1.065* | *931* | *59.1* | |
| T-45 | Two-mica granite | Zhidan | Y | 30°07′ | 90°32′ | 32 | 77.3 | 6 | | | | 15.45 | 0.2273 | 0.512174 | −9.01 | *−9.10* | *1.069* | *932* | *59.2* | |
| T-48 | Two-mica granite | Zhidan | Y | 30°08′ | 90°32′ | 32 | 76.6 | 4 | | | | 13.43 | 0.2298 | 0.512182 | −8.86 | *−8.95* | *1.059* | *929* | *59.0* | |
| QC5 | Two-mica granite | Kapp | Ny | 30°08′ | 90°27.5′ | 10.8 | 73 | 143 | 2.709 | 0.72225 | 0.72148 | 25.59 | 0.1156 | 0.512202 | −8.47 | −8.26 | 1.016 | 916 | 57.8 | |
| QC11A | Two-mica granite | Kapp | Ny | | | 20 | | 113 | 4.396 | 0.71143 | 0.71018 | 21.90 | 0.1101 | 0.512220 | −8.11 | −7.90 | 0.994 | 908 | 57.2 | |
| ND-4-00 | Two-mica granite | Kapp | Ny | 30°21.5′ | 90°20.5′ | 20 | 70.9 | 41 | 39.085 | 0.71981 | 0.70871 | 11.47 | 0.1255 | 0.512315 | −6.26 | −6.08 | 0.880 | 863 | 53.3 | 21.73 |
| BD-3-00 | Biotite-granite | Kapp | Ny | 30°17.5′ | 90°35.3′ | 20 | 74.3 | 144 | 14.69 | 0.71597 | 0.71180 | 41.20 | 0.1283 | 0.512278 | −6.98 | −6.81 | 0.926 | 883 | 55.0 | 25.52 |
| BD-7-00 | Two-mica-granite | Kapp | Ny | 30°17.8′ | 90°35.0′ | 9 | 73.1 | 336 | 53.18 | 0.71493 | 0.70813 | 25.80 | 0.1929 | 0.512278 | −6.98 | −6.98 | 0.936 | 887 | 55.3 | 32.69 |
| BD-8-00 | Biotite-granite | Kapp | Ny | 30°17.8′ | 90°36.8′ | 9 | 78.8 | 97 | 3.91 | 0.71369 | 0.71319 | 18.00 | 0.1001 | 0.512208 | −8.35 | −8.24 | 1.015 | 915 | 57.8 | |
| QC2 | Biotite-granite | Kapp | Ny | 30°13.0′ | 90°21′ | 17 | 72.8 | 122 | 7.85 | 0.71431 | 0.71242 | 98.50 | 0.0994 | 0.512260 | −7.33 | −7.13 | 0.946 | 891 | 55.6 | 56.89 |
| QC4 | Two-mica-granite | Kapp | Ny | 30°10.4′ | 90°25.5′ | 9 | 76.8 | 37 | 26.03 | 0.75283 | 0.74950 | 7.50 | 0.1854 | 0.512250 | −7.53 | −7.52 | 0.970 | 900 | 56.4 | |
| QC7 | Biotite-granite | Kapp | Ny | | | | | | 7.55 | 0.70958 | 0.70744 | | 0.1067 | 0.512260 | −7.33 | −7.11 | 0.944 | 890 | 55.6 | |
| QC8 | Granodiorite | Kapp | Ny | | | | | | 5.53 | 0.71398 | 0.71241 | | 0.1244 | 0.512310 | −6.36 | −6.18 | 0.886 | 866 | 53.5 | |
| QC14 | Biotite-granite | Kapp | Ny | 30°18.5′ | 90°33.0′ | 18 | 68.9 | 290 | 4.34 | 0.70791 | 0.70680 | 49.30 | 0.0773 | 0.512370 | −5.19 | −4.92 | 0.808 | 829 | 50.4 | 13.83 |
| QC17 | Granite | Kapp | Ny | 30°17.5′ | 90°35.4′ | 21 | 74.3 | 106 | 10.7 | 0.71155 | 0.70851 | 25.90 | 0.1284 | 0.512320 | −6.16 | −5.99 | 0.874 | 861 | 53.1 | |
| QC18 | Biotite-granite | Kapp | Ny | 30°17.5′ | 90°36.1′ | 22 | 74.4 | 113 | 8.58 | 0.71125 | 0.70881 | 21.80 | 0.1284 | 0.512250 | −7.53 | −7.36 | 0.960 | 896 | 56.1 | |
| QC19 | Biotite-granite | Kapp | Ny | 30°17.5′ | 90°36.2′ | 22 | 75 | 57 | 20.92 | 0.71305 | 0.70711 | 20.60 | 0.1555 | 0.512310 | −6.36 | −6.26 | 0.891 | 868 | 53.7 | |
| Jm-16 | Adakitic granite | Hou et al | J | 29.67 | 91.72 | 15 | 68.3 | 239 | 4.206 | 0.70792 | 0.70702 | 19.16 | 0.0942 | 0.512559 | −1.50 | −1.31 | 0.665 | 748 | 43.8 | 27.05 |
| Jm-23 | Adakitic granite | Hou et al | J | 29.67 | 91.72 | 15 | 68 | 282 | 4.791 | 0.70736 | 0.70634 | 19.44 | 0.0919 | 0.512565 | −1.38 | −1.19 | 0.656 | 742 | 43.3 | 36.44 |
| Jmy-01 | Adakitic granite | Hou et al | J | 29.67 | 91.72 | 15 | 68.6 | 444 | 2.238 | 0.70736 | 0.70688 | 19.86 | 0.0912 | 0.512511 | −2.44 | −2.24 | 0.731 | 788 | 47.0 | 35.72 |
| Jmy-04 | Adakitic granite | Hou et al | J | 29.67 | 91.72 | 15 | 67.1 | 267 | 4.403 | 0.70754 | 0.70660 | 22.41 | 0.0927 | 0.512313 | −6.30 | −6.10 | 1.007 | 913 | 57.5 | 37.02 |
| Jmy-07 | Adakitic granite | Hou et al | J | 29.67 | 91.72 | 15 | 68.1 | 409 | 2.598 | 0.70703 | 0.70648 | 19.94 | 0.0772 | 0.512517 | −2.32 | −2.09 | 0.721 | 781 | 46.5 | 31.66 |
| Dzl-07 | Granite | Hou et al | L | 29.5 | 91.32 | 13 | 71.5 | 570 | 2.031 | 0.70520 | 0.70483 | 21.80 | 0.0950 | 0.512733 | 1.89 | 2.06 | 0.424 | 570 | 30.2 | 32.61 |
| Dzl-06 | Granite | Hou et al | L | 29.5 | 91.32 | 13 | 70.1 | 490 | 0.44 | 0.70516 | 0.70508 | 14.30 | 0.0983 | 0.512680 | 0.86 | 1.02 | 0.499 | 630 | 34.7 | 26.87 |
| Dzl-05 | Granite | Hou et al | L | 29.5 | 91.32 | 13 | 71.3 | 656 | 0.39 | 0.70515 | 0.70507 | 16.60 | 0.0952 | 0.512728 | 1.79 | 1.96 | 0.431 | 576 | 30.6 | 26.36 |
| Dzl-01 | Granite | Hou et al | L | 29.5 | 91.32 | 13 | 72.4 | 348 | 1.03 | 0.70544 | 0.70525 | 16.60 | 0.0999 | 0.512662 | 0.51 | 0.67 | 0.524 | 650 | 36.1 | 26.88 |
| Nmy-07 | Granite | Hou et al | Na | 29.4 | 90.8 | 16 | 70.1 | 501 | 0.76 | 0.70504 | 0.70487 | 12.60 | 0.1029 | 0.512920 | 5.54 | 5.73 | 0.162 | 320 | 13.2 | 23.99 |
| Nmy-04 | Granite | Hou et al | Na | 29.4 | 90.8 | 16 | 71.2 | 523 | 0.561 | 0.70528 | 0.70515 | 15.23 | 0.0961 | 0.512740 | 2.03 | 2.23 | 0.412 | 560 | 29.5 | 30.49 |
| PI-18 | Granite | Hou et al | Na | 29.4 | 90.8 | 16 | 68.4 | 469 | 0.299 | 0.70506 | 0.70500 | 15.60 | 0.0945 | 0.512716 | 1.56 | 1.77 | 0.445 | 588 | 31.5 | 19.13 |
| PI-28 | Granite | Hou et al | Na | 29.4 | 90.8 | 16 | 66.5 | 500 | 0.622 | 0.70532 | 0.70517 | 29.40 | 0.0926 | 0.512651 | 0.29 | 0.50 | 0.536 | 659 | 36.8 | 40.15 |
| Ng-16 | Granite | Hou et al | Na | 29.4 | 90.8 | 16 | 68.5 | 729 | 0.194 | 0.70513 | 0.70508 | 18.90 | 0.0818 | 0.512459 | −3.45 | −3.22 | 0.801 | 826 | 50.1 | 34.14 |
| Ng-18 | Granite | Hou et al | Na | 29.4 | 90.8 | 16 | 68.8 | 685 | 0.236 | 0.70491 | 0.70485 | 17.50 | 0.0940 | 0.512702 | 1.29 | 1.50 | 0.464 | 603 | 32.6 | 35.20 |
| Cj-02 | Granite | Hou et al | Ni | 29.5 | 90 | 15 | 68.9 | 118 | 5.849 | 0.70642 | 0.70518 | 18.10 | 0.0918 | 0.512679 | 0.84 | 1.04 | 0.497 | 629 | 34.6 | 32.27 |
| Cj-20 | Granite | Hou et al | Ni | 29.5 | 90 | 15 | 64.9 | 309 | 1.586 | 0.70560 | 0.70526 | 18.80 | 0.0970 | 0.512529 | −2.09 | −1.90 | 0.707 | 773 | 45.9 | 32.11 |
| Cj-22 | Granite | Hou et al | Ni | 29.5 | 90 | 15 | 67.9 | 290 | 0.76 | 0.70575 | 0.70558 | 16.00 | 0.0952 | 0.512568 | −1.33 | −1.13 | 0.652 | 739 | 43.1 | 28.91 |
| Nt-03 | Granite | Hou et al | Ni | 29.45 | 90.05 | 16.5 | 67.9 | 686 | 0.566 | 0.70556 | 0.70543 | 25.59 | 0.1100 | 0.512630 | −0.12 | 0.06 | 0.567 | 682 | 38.6 | 18.80 |
| Nt-08 | Granite | Hou et al | Ni | 29.45 | 90.05 | 16.5 | 66.8 | 586 | 0.598 | 0.70580 | 0.70566 | 19.75 | 0.0967 | 0.512529 | −2.09 | −1.88 | 0.706 | 773 | 45.8 | 37.86 |
| Nt-10 | Granite | Hou et al | Ni | 29.45 | 90.05 | 16.5 | 68.2 | 637 | 1.383 | 0.70626 | 0.70593 | 25.90 | 0.0972 | 0.512563 | −1.42 | −1.22 | 0.659 | 743 | 43.4 | 37.45 |

M = Marjiang Pass; Y = Yanbajing; Ny = Nyangentangla Range; J = Jiama; L = Lakang'e; Na = Nanmu; Ni = Nimu.
[a] NCI calculated using crustal epsilon Nd value of −8 for Latitude north of 30°N°N, −6 south of 30°N, +8 for mantle value.
[b] $T_a$ = assimilation temperature and h = crustal thickness; see Appendix.

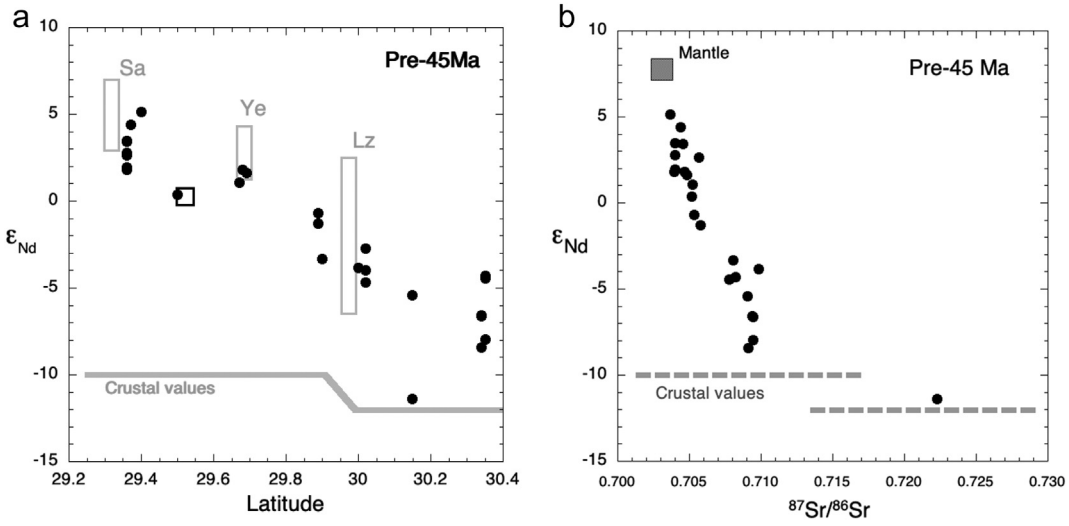


**Fig. 2.** (a) Nd isotopic data from pre-45 Ma granitoids versus latitude. Also shown are the range of values for the Sangri (Sa), Yeba (Ye) and Linzizong (Lz) volcanic sequences. (b) Nd versus Sr isotope ratios. Crustal $\varepsilon_{Nd}$ values, estimated from metasedimentary samples and two-mica granites, are −10 south of 29.9°N and −12 north of that latitude.

formation, and hence complement the two-mica granites that reflect the deeper crust. The metasedimentary samples measured span the north-south range from just south of Lhasa to just north of the IYS. We analyzed 7 samples, mostly meta-shale and meta-siltstone that have zircon populations suggesting Cretaceous and Late Jurassic sedimentation ages (Table 3), with one exception that is presumably contaminated with younger material since it occurs within the same section and at the same locality as other samples that give Cretaceous ages. The measured $\varepsilon_{Nd}$ values are between −12.1 and −8.9 with an average of −10.3 (Fig. 4). These values are close to, but slightly higher than, the values of the Juassic peraluminous granites from farther north, which are −12 to −13. Hence, the available evidence indicates that the crustal rocks that pre-date the early Cenozoic intrusives and could act as contaminants for mantle-derived magmas, crystalline basement north of 29.8°N and a relatively thick clastic sedimentary sequence (presumably deposited on oceanic crust or thin continental crust) south of 29.8°N, had a restricted range of $\varepsilon_{Nd}$ values at the time of batholith formation between about −10 and −12, with a slight shift of about 2–3 $\varepsilon_{Nd}$ units from south to north.

Mid-Cenozoic (30 Ma) two-mica granites occur in the Yangbaijan area, and have $\varepsilon_{Nd}$ values of about $-8 \pm 1.5$, significantly higher than the Jurassic granites (Table 2; Fig. 4). These rocks suggest that the southern Lhasa Block basement was modified between Jurassic and mid-Cenozoic time, possibly by addition of mantle derived magma, or that there is an age province boundary at about latitude 30.3°N between slightly younger and older Proterozoic basement. We take the $\varepsilon_{Nd}$ values of the 30 Ma two-mica granites to represent the post-32 Ma basement. The basement $\varepsilon_{Nd}$ values for the 45–62 Ma granite suite are bracketed by the Jurassic and mid-Cenozoic two-mica granites to be between −8 and − 12. For the crustal thickness calculations we assume that the crustal component for the 45–62 Ma granitoids north of 30°N latitude has $\varepsilon_{Nd} = -12$ and the crustal component south of 30°N has $\varepsilon_{Nd} = -10$ (Fig. 2).

In addition to the continentally-derived metasediments the pre-batholithic wallrocks also contain volcanic sections. The Yeba sequence that is exposed east of Lhasa (Fig. 1), has $\varepsilon_{Nd}$ values in the range of +1 to +4 in mafic and intermediate volcanic rocks (Zhu et al., 2008; Fig. 2). Close to the suture, the Sangri volcanic sequence has $\varepsilon_{Nd}$ values in the

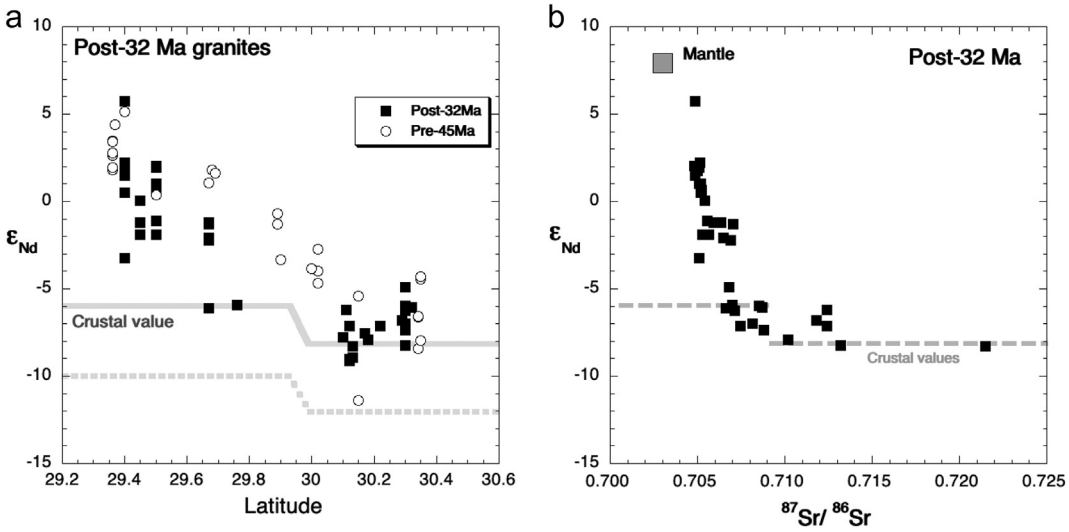


**Fig. 3.** (a) Nd isotopic data from post-32 Ma granitoids versus latitude. (b) Nd versus Sr isotope ratios showing inferred crustal values of $\varepsilon_{Nd}$ south of 29.9°N (−6) and north of that latitude (−8).

**Table 3**
Age and isotopic data for prebatholithic metasedimentary rocks.

| Number | Rock type | Latitude | Longitude | Age (Ma)* | Nd | Sm | Sr | Rb | Hf[a] | $\varepsilon_{Nd}$(m) | $^{87}Sr/^{86}Sr$ | $\varepsilon_{Hf}$ (m)[a] | $^{147}Sm/^{144}Nd$ | $\varepsilon_{Nd}$ (50) | $^{87}Sr/^{86}Sr$(50) |
|---|---|---|---|---|---|---|---|---|---|---|---|---|---|---|---|
| 14DLB47A | Schist | N29°22′59.2" | E91°49′51.8" | 120 | 29.2 | 5.32 | 97 | 182 | 4.5 | −10.2 | 0.71944 | −4.90 | 0.1102 | −9.65 | 0.71559 |
| 14DLB47B | Schist | N29°23′01.2" | E91°49′55.2" | 121 | 32.3 | 5.15 | 146 | 122 | 5.21 | | | | 0.0964 | | |
| 14DLB47C | Schist | N29°23′04.1" | E91°49′58.7" | 120 | 29.2 | 4.99 | 139 | 138 | 4.48 | −8.85 | 0.71606 | −2.93 | 0.1034 | −8.26 | 0.71402 |
| 14DLB47D | Schist | N29°23′12.8" | E91°49′57.2" | 118 | 36.3 | 7.31 | 154 | 132 | 4.26 | | | | 0.1218 | | |
| 14DLB47E | Schist | N29°23′16.3" | E91°49′56.0" | 148 | 29.7 | 5.72 | 108 | 139 | 5.59 | −9.57 | 0.71623 | −9.90 | 0.1165 | −9.06 | 0.71358 |
| 14DLB48 | Schist | N29°28′56.3" | E91°50′25.9" | | 23.3 | 4.43 | 441 | 94.3 | 3.09 | −10.51 | 0.70956 | −9.08 | 0.1150 | −9.99 | 0.70912 |
| 14DLB49 | Volcanic schist | N29°23′01.5" | E92°01′34.8" | | 10.7 | 3.03 | 51.9 | 56.4 | 3.22 | 5.71 | 0.70832 | 13.16 | 0.1713 | 5.87 | 0.70609 |
| 14DLB53 | Schist | N29°37′19.1" | E91°04′29.5" | | 22.8 | 4.96 | 44 | 82.9 | 5.12 | −12.09 | 0.72943 | −18.12 | 0.1316 | −11.68 | 0.72556 |
| 14DLB54 | Sandy lens in shale | N29°37′17.5" | E91°04′27.2" | 178 | 12.2 | 2.68 | 22.6 | 35 | 4.23 | −11.9 | 0.72589 | −21.52 | 0.1329 | −11.50 | 0.72271 |
| 14DLB55 | Siltstone/marl | N29°33′05.4" | E92°02′31.0" | | 34.1 | 6.67 | 127 | 180 | 4.53 | −9.12 | 0.71526 | −3.94 | 0.1183 | −8.62 | 0.71235 |

[a] Age determined by multiple zircon U—Pb determinations by LA-ICPMS at CUG Wuhan; Hf concentration and isotopes measured at the PCIGR laboratory at U. British Columbia.

range +3 to +7 (Kang et al., 2014; Fig. 2). These volcanic sequences are not large in volume and occupy the uppermost crust. Their isotopic characteristics suggest that the mantle magma sources available for the convergent margin magmatism had high, positive $\varepsilon_{Nd}$ values. It is possible that lower crustal $\varepsilon_{Nd}$ values in the areas where these volcanic sequences occur are slightly higher due to this volcanic activity, but our baseline model assumes that their presence does not significantly affect the crustal $\varepsilon_{Nd}$ value.

## 4. Geochemical approaches to estimating paleo-crustal thickness

Our approach to using granite Nd isotopic data as a crustal thickness probe, described in detail in the Appendix, involves models of magmatic assimilation and recharge that apply to the mechanism of formation of the granitic magmas. DePaolo (1985), DePaolo et al. (1992) and Perry et al. (1993) developed a framework relating Nd isotopes in granitic and rhyolitic igneous rocks to crustal temperature structure that was later refined by Jellinek and DePaolo (2003) and used by Hammersley and DePaolo (2006). In this model, high wallrock temperature enhances crustal assimilation by permitting more of the introduced juvenile heat from the magma to be used to melt (and incorporate), rather than raise the temperature of, surrounding wallrock. The Nd isotopic data, therefore, can be viewed as providing information about the temperature of the crustal region at which the bulk of crustal assimilation occurs. The isotopes of Hf, Sr and Pb also provide indications of crustal involvement in granitoid magmatism, but for our purposes Nd isotopes provide sufficient information and fewer complications and hence we restrict our quantitative analysis to them. Strontium isotopes provide additional useful constraints to supplement the Nd isotopes, and to a large extent Hf isotopes parallel Nd isotopes where data are available (cf. Chapman et al., 2017). It has also been demonstrated that La/Yb and Sr/Y trace element ratios in granitoids provide a good reflection of crustal thickness at the time of magmatism (Profeta et al., 2015; Farner and Lee, 2017). In subduction-related granitoids this relationship arises in a manner that is broadly similar to that inferred for Nd isotopes, although the signal is not dependent on the age of the crustal rocks involved. An updated description of the Nd isotope model is provided in the Appendix; the models relating to La/Yb and Sr/Y are discussed in detail in Farner and Lee (2017). Hu et al. (2017) have proposed an extension of the La/Yb approach to collisional granites and their relationship is used here for the post-32 Ma granites.

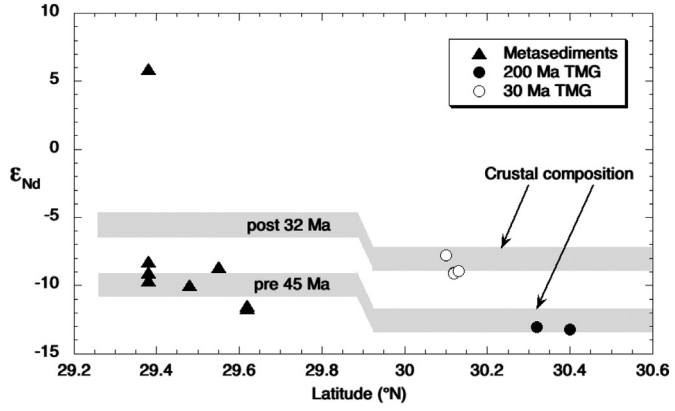


**Fig. 4.** Nd isotopic values ($\varepsilon_{Nd}$) of Cretaceous metasedimentary rocks and 30 Ma two-mica granites used to define the composition of the crustal component for the assimilation-recharge model. The $\varepsilon_{Nd}$ values are calculated to an age of 50 Ma. One sample with high $\varepsilon_{Nd}$ is a volcanogenic phyllite. The grey shaded zones are the values used for the crustal thickness estimates; the $\varepsilon_{Nd}$ values are inferred to be slightly different north and south of 29.9°N.

The assimilation model for Nd isotopes provides a temperature, not specifically a depth, of the level in the crust where the bulk of assimilation takes place. The expectation is that this "effective assimilation temperature" applies to the lowermost crust near the Moho. This expectation stems from the fact that the thermodynamically allowed rate of assimilation is sensitive to wallrock temperature (DePaolo, 1985; DePaolo et al., 1992) and hence will be a maximum just above the Moho where crustal rocks are generally the hottest. The second consideration is that the large density contrast at the Moho means that upward moving magma is likely to stall near the Moho until differentiation (±assimilation) lowers the density sufficiently for the magma to move up into the mid- to upper crust. Since there is a slightly extended residence near the Moho, and a need for differentiation to decrease density, it is consistent for these reasons to expect that most of the crustal assimilation occurs there as well. However, since it is required that the mean depth of the assimilation is somewhat shallower than the Moho, estimates of crustal thickness based on the Nd isotope approach are, strictly speaking, lower limits, but perhaps within 5–10 km of the full crustal thickness.

The La/Yb approach as applied to subduction-related granitoids is based on similar considerations as the Nd isotope approach. Mantle – derived magmas tend to have relatively low normalized La/Yb. Crustal rocks have considerably higher La/Yb. In a model magma chamber as conceptualized for the Nd isotope approach, assimilation of crustal rocks accompanied by fractional crystallization will cause the magma La/Yb to increase. However, whereas fractional crystallization does not change the Nd isotope ratio, it does tend to increase the La/Yb ratio, enhancing the effects of assimilation, and hence creating ambiguity about the role of crustal melting. A further dependence on crustal thickness comes from mineralogical considerations, since at high enough pressure garnet becomes a stable liquidus phase, and its partitioning of rare earth elements is such that its presence causes further increase of magmatic La/Yb (Farner and Lee, 2017). The La/Yb approach also implicitly assumes that the critical magmatic processes take place near the Moho, and/or integrate over a distance related to the thickness of the lower crust, and hence reflect crustal thickness.

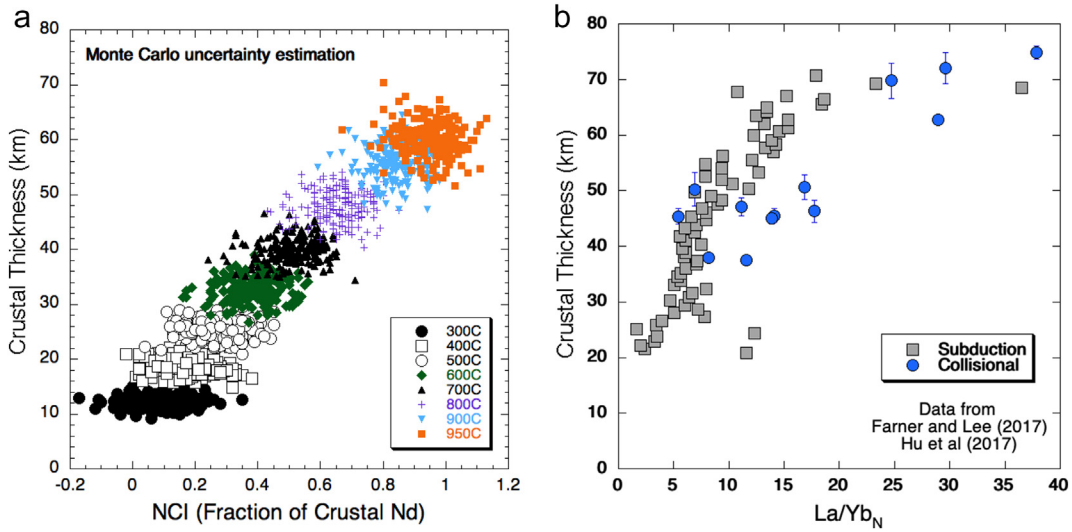


**Fig. 5.** Crustal thickness estimates as related to Neodymium Crustal Index (NCI) and to chondrite-normalized La/Yb. (a) Relationship of thickness to NCI shown with approximate uncertainty estimate from a Monte Carlo approach where temperature is specified and all other parameters are allowed to vary within specified limits (details in appendix). (b) Crustal thickness as related to observed, aerially averaged La/Yb$_N$ of granitoids with $SiO_2$ between 54 and 68%. Subduction-related granites from Farner and Lee (2017) and collisional granites from Hu et al. (2017). The data in panel b include samples from Tibet, but those are younger than the granites discussed in this study.

A summary of the relationships between NCI (Nd isotopes), La/Yb, and crustal thickness is provided in Fig. 5. The relationships for La/Yb, although broadly justifiable theoretically, are empirical and derived from observations of intrusive and volcanic rock geochemistry in regions where crustal thickness, or elevation, has been measured or can be reasonably inferred (Farner and Lee, 2017; Hu et al., 2017). The relationship for NCI has not been confirmed with a global dataset, but is developed from theoretical models as detailed in the Appendix. The results presented here provide initial confirmation that the Nd isotope approach yields results that are consistent with those from La/Yb. The La/Yb method requires that the granitoids being considered have a limited range of $SiO_2$ between about 54 and 68% by weight. The Nd isotope approach does not have this limitation, and we have used Nd isotope data from many high-$SiO_2$ granites. The Nd isotope method as we have formulated it saturates at a crustal thickness of about 60 km (this limit is a function of the assumed magma temperatures), and the La/Yb approach saturates at a crustal thickness of about 70 km (Fig. 5).

### 4.1. Nd isotope crustal thickness estimates

We derive the pre-collision crustal thickness profile shown in Fig. 6a from the Nd isotopic data on the pre-45 Ma granitoids. As noted above, the model is sensitive to crustal thickness when thickness is less than ~60 km. Our model results indicate that the crust of the Lhasa Block that is now located within 50–60 km of the IYS, was thin, with an estimated thickness of 25–35 km until at least 45 Ma. The data also suggest that north of about 29.9°N, the crust was thicker, in the range 50–60 km. There is some evidence for a jump in thickness at about 29.9°N latitude, which might constitute the location of the edge of thick crystalline crust of the Lhasa Block at ca. 50 Ma.

Granitoids that are emplaced post-21 Ma (and one that is 30 Ma), have substantially lower $\varepsilon_{Nd}$ values in the region between the IYS and about 29.8°N latitude (Fig. 3b). This indicates that the crust in this region was modified relative to the pre-45 Ma crust. We assume that the earlier magmatism resulted in a substantial addition of mantle

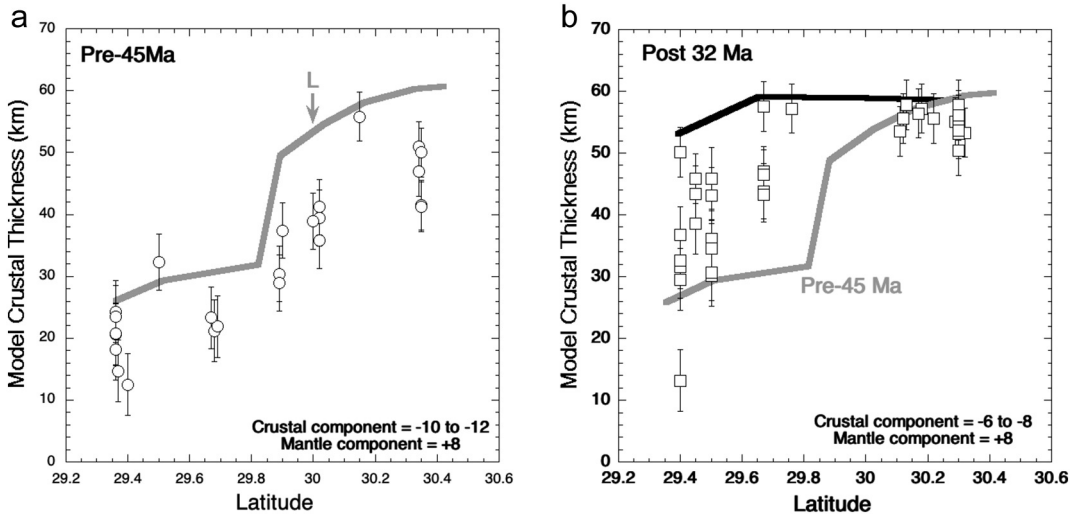


**Fig. 6.** Crustal thickness profile of southern Lhasa Block near the longitude of Lhasa inferred from Nd isotopes and assimilation-recharge model. (a) Profile (grey line) based on Nd isotopic compositions of pre-45 Ma granitoids. The letter "L" indicates the latitude of samples of sampled Linzizong volcanic rocks. (b) Thickness profile (black line) inferred from post-32 Ma granitoids.

derived (i.e., high $\varepsilon_{Nd}$) magma to the lower crust, and hence led to a significant increase in the average lower crustal $\varepsilon_{Nd}$, from an original value of about −10, to a new value of −6. This value is chosen to be somewhat higher than the value of about −8 found for granites north of 29.9°N, because it is likely that the Late Cretaceous and Early Cenozoic magmatism had more effect in this region closer to the modern suture where magma fluxes were likely to be higher.

The calculations for the post-21 Ma granites (Fig. 6b) indicate that the crust in the region south of 29.8°N had thickened from 25 to 35 km at 45 Ma to 50–60 km by 21 Ma. The crust north of 29.8°N appears to have remained thick, at least 55–60 km but there is no evidence that it became thicker over the time interval between 45 and 32 Ma. Hence the Nd isotope model suggests markedly non-uniform thickening over this 150 km wide swath of southern Tibet, with 20–30 km of thickening in the region between the YTS and 29.8°N, and little thickening north of 29.9°N in the same time period.

### 4.2. Crustal thickness estimates from La/Yb ratios

The available data on La/Yb, grouped into the similar age ranges as those of the Nd data, and taken from an area slightly broader than those of the Nd isotope data, are shown in Fig. 7. The data are from the database compiled by Chapman and Kapp (2017) with the addition of data from the rocks reported on here. The plotted data are restricted to rocks with $SiO_2$ contents > 60% and <68% The approximate inferred crustal thickness is taken from the compilations of Farner and Lee (2017) and Hu et al. (2017) as summarized in Fig. 5. La/Yb is less sensitive to differences in crustal thickness in the range of 25–45 km, but can clearly indicate when crustal thickness exceeds about 50 km. The La/Yb data are consistent with the inferences from Nd isotopes for the older (>45 Ma) granite suite, except for a small number of samples that have higher La/Yb (e.g. Ji et al., 2011). The preponderance of data from south of 29.8°N indicate relatively thin crust, in the range of 30–40 km, close to the estimates from Nd isotopes (Fig. 6a). North of 29.8°N the indicated crustal thickness values are in the 60–65 km range, also consistent with the Nd data although there are few Nd data in that latitude range.

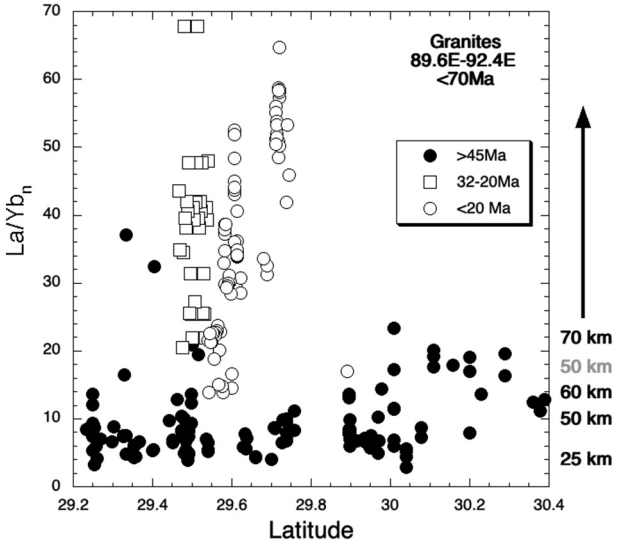


**Fig. 7.** Chondrite-normalized La/Yb ratios from granitic rocks with 54% < $SiO_2$ < 68% from the study area. Data include those from Tables 1 and 2 plus additional samples from the database of Chapman and Kapp (2017); see table in Appendix). Thickness scale on the right in bold black type is taken from the compilation of Farner and Lee (2017) and applies to the pre-45 Ma granitoids. Grey "50 km" corresponds roughly to the estimate for collisional granites from Hu et al. (2017) and applies to post-32 Ma granitoids (Fig. 5). Values of $La/Yb_N$ > 20 to 25 are indicative of crustal thickness of approximately 70 km for both groups of granitoids (Fig. 5).

There are enough La/Yb data on granitoids with ages < 32 Ma that they can separated into two age groups, 32–20 Ma and <20 Ma. These younger granites are mostly restricted to the latitude range of 29.5 to 29.8°N and all show extremely high La/Yb indicative of crustal thickness values that are >60 km and mostly about 70 km. Both the La/Yb data and the Nd isotope data clearly show a contrast between rocks with ages >45 Ma and those with ages of 32 Ma or less. Thus, both approaches appear to bracket the time of major thickening of the crust of the southern Lhasa Block margin to between 45 and 32 Ma. The Nd data give values that are somewhat lower than those derived from La/Yb. This is the expected direction of difference given that the assumptions in the Nd isotope model tend to cause the estimates to err on the low side. The Nd isotope model gives values that are close to those of La/Yb for thinner crust, but low by up to about 10 km for thick (>50 km) crust. In the range of crustal thickness between 25 and 45 km, the Nd isotope approach may provide more resolution than La/Yb.

## 5. Eocene ignimbrites and lake carbonate deposits

In addition to the granitic magmatism in early Cenozoic time, the region just north of the latitude of Lhasa was also affected by widespread explosive volcanism resulting in substantial accumulations of silicic ignimbrites (Mo et al., 2007; Lee et al., 2012), the Linzizong sequence. These rocks also provide isotopic indications of crustal thickness at the time they were forming in the early Eocene. There are in addition, data on paleo-elevation based on stable isotope compositions of lacustrine carbonates that formed contemporaneously with the ignimbrites (Ding et al., 2014; Ingalls et al., 2017).

The range of $\varepsilon_{Nd}$ values of the Linzizong silicic ignimbrites from the Linzhou Basin are shown in the $\varepsilon_{Nd}$ vs latitude plot in Fig. 2. The values span the range −7 to +2. The lower range of the ignimbrite values are similar to those of granites at the same latitude. The upper limit provides evidence that the $\varepsilon_{Nd}$ of the mantle magma sources was higher than +2, and considering that even those values probably include crustal contamination, are consistent with there being high $\varepsilon_{Nd}$ (likely greater than +5) mantle magma entering the crust at the latitude of the Linzhou basin (30.0°N where most of sampling was done). There is one $\varepsilon_{Nd}$ value reported that is as high as +9 (Mo et al., 2008). Because *eruptible* magma is expected to require lower *a*/*r* values and have slightly higher $\varepsilon_{Nd}$ than intrusive magma mushes, the $\varepsilon_{Nd}$ of the Linzizong ignimbrites provides confirmation of the inference about crustal thickness based on the granitoids (thickness at least 50–55 km) at this latitude. Furthermore, estimates of paleo-elevation based on stable isotope compositions of lacustrine carbonates, which range from 3200 to >4500 m for the Linzhou Basin (Ding et al., 2014; Ingalls et al., 2017), correspond to likely crustal thickness of 55 to 65 km. This range is also compatible with the inferences from Nd isotopes and La/Yb that crustal thickness was 55–65 km (Fig. 6). The paleoelevation data provide a rough calibration point for the conversion of granite Nd isotopic compositions to crustal thickness and shows consistency with the inferences from La/Yb ratios. The inferred crustal thickness of >50–55 km accords with observations in the Central Andes where large volume Late Cenozoic ignimbrites, with uniformly high NCI values similar to those observed for the Linzizong sequence, are restricted to areas with crustal thickness ≥ 50 km (e.g. Kay et al., 2010; Mamani et al., 2008; McGlashan et al., 2008). Ding et al. (2014) also noted the similarities between the Eocene structure and magmatism of the Lhasa Block and the modern central Andes.

## 6. Magma sources and crustal assimilation

An underlying assumption of our models of magma genesis and the relation to Nd isotopes is the involvement of preexisting continental crustal material (with low $\varepsilon_{Nd}$ and relatively high Nd concentration) in the generation of granitic magmas. This concept has been developed over an extended period and is supported by data from numerous

granitic and rhyolitic rocks (DePaolo, 1981; Hildreth, 1981; Farmer and DePaolo, 1983; Hildreth and Moorbath, 1988; Borg et al., 1990; Mamani et al., 2008, 2010). The model as we have implemented it also carries the assumption that the $\varepsilon_{Nd}$ of mantle magma sources is not highly variable in arc settings, with values between about +5 and + 9 being nearly universal. Such high $\varepsilon_{Nd}$ of mantle magma sources under southern Tibet is supported by the observation of high $\varepsilon_{Nd}$ values in volcanic rocks (Fig. 2). Low $\varepsilon_{Nd}$ values in granites are therefore inferred to be due to assimilation or magma mixing involving continental crustal rocks that have much lower $\varepsilon_{Nd}$ of −6 to −12. The conclusions we reach with this approach are consistent with other geochemical parameters (La/Yb) and with paleoelevation studies that indicate crustal thickness as discussed above.

An alternative hypothesis, favored by Chapman et al. (2017) for example, is that crustal involvement in magma genesis does not vary systematically, but rather the isotopic composition of mantle magma sources changes. They cite in support of this model the low $\varepsilon_{Nd}$ values measured in Eocene and younger mafic alkaline volcanic rocks from several areas of southern Tibet (Zhao et al., 2009). These rocks clearly provide evidence of the existence of mantle with low $\varepsilon_{Nd,}$ but they have another characteristic – miniscule volumes of erupted magma - that suggests that they are not necessarily relevant to the problem of large-scale granitic magma genesis. The rocks of the Gangdese batholith over the extent of the study area (Fig. 1) constitute a total volume of magma that could be roughly estimated as 150,000 $km^3$ (25 $km^3$/Myr/km of arc x 30 Myr × 200 km of arc). The total amount of magma generated from the mantle is likely to be at least twice this number, or perhaps 300,000 to 400,000 $km^3$. In contrast, the total volume of alkaline magma erupted in the same length of time, although not tightly constrained by descriptions in the literature, is of order 10–100 $km^3$, or >1000 times smaller than the amount of granitic parental magma. Whereas there are mechanisms that can generate alkaline basaltic magmas from continental lithosphere, in small amounts and generally in extensional environments, there are no mechanisms for melting the lithosphere in sufficient volumes and at sufficient rates to generate large batholithic accumulations of granitic magma. The magma sources of the alkaline rocks probably represent a volumetrically tiny fraction of the subcontinental mantle that happens to be enriched in incompatible elements and have crustal-type Nd isotopic characteristics. It is these anomalous enriched enclaves in the lithosphere that can melt in the absence of a major thermal-convective perturbation of the type necessary to generate a continental margin arc. Incorporation of some of this enriched lithospheric material into asthenospheric melts might be expected, but the volumes are too small to account for the regional variations in granite isotopic compositions.

One further aspect of the crustal assimilation model, which is to some degree misrepresented by Chapman et al. (2017), is that because almost all assimilation or magma mixing takes place in the lower crust and involves the input of basaltic magma from the mantle, it is not expected that this assimilation process would lead to an overall correlation between $SiO_2$ content and $\varepsilon_{Nd}$. This point is discussed in Perry et al. (1993), DePaolo et al. (1992) and Hammersley and DePaolo (2006). Most of the shift of isotopic composition due to assimilation takes place in a range of $SiO_2$ between about 49 and 56 wt%, so that even the more mafic components of the batholiths (and the mafic enclaves in granodiorites) show most of the assimilation signal. The fact that more mafic components exhibit the large isotopic variations (Chapman et al., 2017) is a feature of the assimilation model rather than an argument against it.

There is, however, a question as to whether the assimilation-recharge model is applicable to post-collision granites. It has been suggested that post-collisional granitoids in southern Tibet were generated ultimately by mantle magma (Gao et al., 2007), which would suggest that the model would apply. Others have suggested that post-collision granitic magmas formed by melting of lower crust that had been highly modified by earlier magmatism (e.g., Hou et al., 2004). For lower crustal melting, the $\varepsilon_{Nd}$ values of the granites would simply reflect those of the lower crust, which is problematical because the relatively high $\varepsilon_{Nd}$ values, mostly between −2 and +2, with one sample at +5.5, would necessitate mostly mafic lower crust or a very large amount of magmatic underplating. This model might work if the *syn*-collisional crust at the southern edge of Tibet were as thin as our lower estimates of 20–25 km (Fig. 6a), in which case there might have been enough underplating to produce lower crust with an average composition of $\varepsilon_{Nd} \approx 0$.

With regard to mantle magma sources for the post-collision granites, and even for the crustal melting model, there are issues because the time period 32 to 9 Ma is well after collision. If there were intact underthrust Indian continental crust, as suggested by Guillot et al. (2008) and Ding et al. (2016). there is difficulty in constructing a reasonable geodynamic model that would allow access to a mantle magma source. In this regard, it is noteworthy that the $\varepsilon_{Nd}$ values of the granites located south of 29.8°N latitude show no obvious indication of direct melting of underthrust Indian continental crust, which is estimated to have typical $\varepsilon_{Nd}$ values of −13 to −18 (Zhang et al., 2004). Possible resolutions that have been proposed to provide mantle magma are lithospheric delamination or subducted slab breakoff (e.g. Hou et al., 2004; He et al., 2007). Other possible explanations are that east-west extension is responsible for the production of post-collision mantle magma (e.g., Debon et al., 1986) or that the early stages of collision involved steep subduction of the Indian slab (Leech et al., 2005) so that the Tibetan mantle wedge could still be a source of mantle magma and that there was little Indian crust added to the lower crust of southernmost Tibet until some time in the Miocene.

## 7. Magmatic contributions to crustal thickening

Our interpretation of the Nd isotope and La/Yb data is that the southernmost 50–60 km of the Tibetan crust was thin until at least 45 Ma. Magmatic additions from the pre-45 Ma activity should however have caused the crust to thicken even in the absence of any tectonic effects. The amount of thickening that might be expected from 20 m.y. of continental margin arc magmatism can be estimated from typical island arc magma production rates, which are about 25 $km^3$/Myr/km of arc (e.g., Reymer and Schubert, 1984) or somewhat less (Davidson and De Silva, 2000). Estimates of rates for continental margin batholiths are similar, about 25–30 $km^3$/Myr/km of arc for the Coast Batholith of British Columbia (Gehrels et al., 2009). This amount of magma addition distributed over the 50 km width of observed thin crust north of the YTS would produce 0.5 km of thickening per million years. Based on this range of thickening rates, during the period from 60 to 40 Ma, the southern edge of the Lhasa Block could have been thickened by 10 km to perhaps 15 km due to magmatic additions from the subduction system. Mo et al. (2007) arrived at a similar estimate for Gangdese magmatic thickening, although they did not evaluate geographic variations. Similarly Ji et al. (2011) found Hf evidence for crustal thickening during the period from 65 to 34 Ma, although again without reference to geographic position.

The Nd isotopic effect of 10–15 km of magmatic addition would be to shift the average composition of the lower crust to higher $\varepsilon_{Nd}$ values. If 10 km of mantle magma with 12 ppm Nd and $\varepsilon_{Nd} = +8$ were added and mixed with 20 km of pre-existing lower crust with 20 ppm Nd and $\varepsilon_{Nd} = -10$, the resulting modified and mixed lower crust would have $\varepsilon_{Nd}$ of −5.8, approximately the value used for the crustal component for the mixing model applied to the post-32 Ma granites (Figs. 4 and 6b). This calculation shows that it is difficult to shift the average lower crustal $\varepsilon_{Nd}$ by injection of mantle magma into something like a "MASH" zone (Hildreth, 1981; Hildreth and Moorbath, 1988; Annen et al., 2006a, 2006b) unless there is little crust to start, or there is a very large fraction of new material added. For example, to shift the average lower crustal value from −10 to 0 would require about 40 km of mantle magma added to 20 km of pre-existing lower crust.

## 8. Discussion

Our conclusion from the above arguments and calculations is that the southernmost 50–100 km of the Asian crust near the longitude of present-day Lhasa (89.5° to 92.3°E) was thinner than normal continental crust and probably at or below sea level during early Tertiary time prior to and during the early stages of collision. The thickness of the crust may have been systematically thinner to the south and may have been only 25 km thick or less at its southern margin as currently exposed. The extent of such thin crust south of the current location of the YTS is poorly known, but any extension could have been thinner yet.

Our inferences about paleo-crustal thickness of the southern part of the Lhasa Block in the longitude range of our study are summarized in Fig. 8. The thin southern margin of the Asian continental crust apparently persisted through the late stages of the main early Cenozoic pulse of Gangdese magmatism to 45 Ma. Magmatic additions during the interval from 65 to 45 Ma could have thickened the crust by 10–15 km, although the evidence for the amount of thickening is indirect and based on average magma production rates in continental margin arc settings.

Our inferred *syn*-collision crustal thickness profile is similar to that measured for the modern western margin of South America and the Andes between latitude 18°S and 28°S (Fromm et al., 2004; Beck et al., 1996; McGlashan et al., 2008). The near-shore region in South America is close to sea level and crustal thicknesses are between 25 and 35 km over a region about 60–100 km wide including the narrow submarine shelf, before changing abruptly to much greater thicknesses (50 to >70 km) to the east under the Altiplano. Also, Nd isotopic compositions of granitic and volcanic rocks show a discontinuity that corresponds with this crustal thickness change and is quite similar to our observations in southern Tibet (Mamani et al., 2008, 2010), although

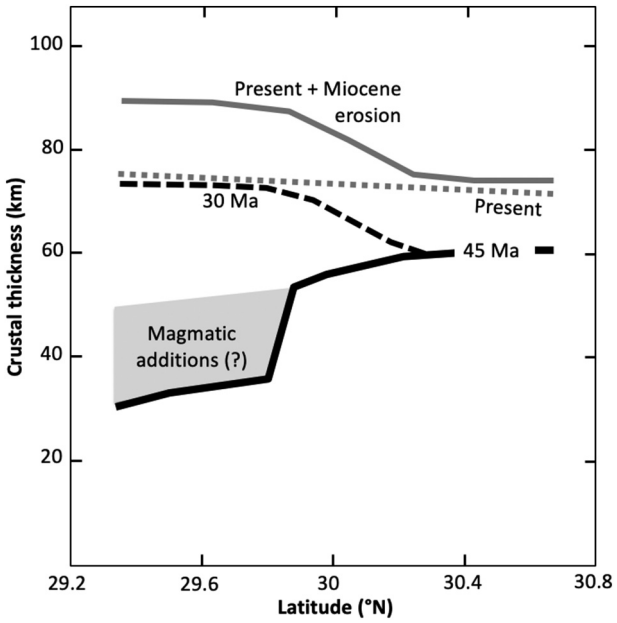


**Fig. 8.** Summary diagram of inferred crustal thickness versus latitude at the longitude of Lhasa (about 91°E). The *syn*-collision southern margin of the Lhasa bock had a stepped thickness profile; thin at the southern margin and extending northward to what is currently 29.8°N. Between 29.8°N and 29.9°N the crustal thickness changed to 50–60 km, an inference based on granite Nd isotopes and La/Yb ratios, and consistent with paleo-elevation studies and the occurrence of widespread Eocene ignimbrites. Between 45 and 30 Ma the region between 29.3° and 29.9°N was dramatically thickened to roughly 70 km, but the region north of 30.2°N may not have been further thickened. Some of the thickening was from magmatic additions, but not most of it. The Miocene erosion profile is based on U,Th-He thermochronometry (Schmidt et al., 2019) and is consistent with the 30 Ma thickness profile shown. Subsequent to 20–30 Ma, there must have been additional uniform further thickening of 10–15 km to account for the present crustal thickness.

the rocks on either side of the discontinuity in South America are not coeval. Our inferred crustal thicknesses North of 30°N (50–60 km) accord well with the modern Andes and the Nd isotopic compositions of the silicic volcanic rocks that are abundant there in regions of similarly thick crust.

The timing of major crustal thickening near the Yarlung-Tsangpo suture is a key conclusion from our study, and is somewhat different from the conclusions reached in previous studies. Zhu et al. (2017), also using La/Yb data, concluded that the crust of the southern Lhasa Block was already thick (but not uniformly) by 50 Ma, but underwent additional thickening between 45 and 30 Ma. By evaluating the data with somewhat finer spatial resolution, we can modify this conclusion. The data as we have analyzed them suggest that the crust within 50–60 km of the suture was still quite thin at 45 Ma, but was dramatically thickened between 45 and 32 Ma. The combined Nd isotope and La/Yb data and models suggest that the crust immediately north of the Y-T suture was thickened from 25 to 35 km to as much as 70–75 km in this relatively narrow time interval. The data of Guan et al. (2012) suggest that the southernmost Lhasa Block crust may have been substantially thickened by 38 Ma. The granite data do not provide all of the spatial coverage we would like since the younger granites are restricted to the latitude interval from 29.4 to 29.75°N and hence do not indicate whether the crust north of 29.8°N was further thickened during this same time interval; the available data provide no evidence that it was.

Combining our results with those of Zhu et al. (2017) plus previous conclusions regarding the timing of uplift of the Himalaya, we propose the following crustal thickening (and likely also elevation) history for the southern-central part of the Himalaya-Tibet region. It should be recognized that these conclusions apply strictly only to the region where we have adequate sample coverage between 89.5°E and 92.5°E longitude and may not be extrapolatable east or west without modifications. Prior to 45 Ma, the southern Lhasa Block crust was thick (>50–55 km) in the region currently between about 29.9°N and 30.5°N latitude, but thin (25–35 km) south of 29.8°N latitude. Between 45 and 32 Ma, the crust in the region south of 29.8°N was thickened from 25 to 35 km to 60–75 km, with or without concomitant further thickening of the crust north of 29.9°N. At 32 Ma, the crustal thickness and elevation of the Himalaya is not well constrained, but most of the activity on the thrust faults that are presumably responsible for the uplift is more recent than 25 Ma. Hence, it is possible that the major mountain range during the 35–25 Ma time window, referred to as the Gangdese Mountains by Zhu et al. (2017), was composed of rocks from the southernmost Lhasa Block. There is however, evidence that the Himalaya became high between 25 and 18 Ma, since that is the time of earliest documented activity on the Main Central Thrust (Yin and Harrison, 2000), and also encompasses the time of formation of the high Himalayan leucogranites (Deniel et al., 1987; Guillot et al., 1994; Harrison et al., 1995; Chen et al., 1996). Recent studies also suggest that, since the erosion of the southern margin of the Lhasa Block slowed markedly by about 10 Ma, the Himalaya probably were high and an effective precipitation barrier by that time (Tremblay et al., 2015). Hence our results, combined with other evidence, suggest that the high topography and thick crust of the southern margin of the Himalaya-Tibet propagated *southward* from ca. 30.5°N to 28.5°N in today's coordinates, about 200 km, between 50 and 20 Ma,. There is no evidence pertaining to how regular this progression was, but the overall average rate of advance was about 5–8 km/Myr.

The inference that the mid-Cenozoic thickening (and uplift) history of the southern Lhasa Block crust was different for the regions south and north of about 29.9°N latitude is consistent with, and could provide an explanation for, recently reported thermochronology results (Schmidt et al., 2019). The thermochronology data suggest that the region north of 29.9°N experienced limited Miocene denudation (≤3 km) whereas the region south of that latitude experienced up to 10 km of denudation, and possibly more close to the modern suture. Additional data will be necessary to evaluate whether the relationships between granite

geochemistry and thermochronology are maintained in other parts of southern Tibet.

A key issue raised by our results is how major crustal thickening in the time period between 45 and 32 Ma could be restricted to the relatively narrow region between the present YT suture and about 30°N. One possibility is that the underthrust Indian lithosphere was being steeply subducted during this time period and not shallowly underplating the Lhasa Block crust, and hence that tectonic accretion was localized in a narrow north-south zone. The transition to shallow subduction may have occurred sometime after the period we suggest there was rapid thickening of the southern Tibet crust. Although some studies have inferred that there was shallow subduction of Indian crust beneath the Lhasa Block as early as 50 Ma (DeCelles et al., 2002; Guillot et al., 2008; Ding et al., 2016), it is not clear how such models can be consistent with the large amount granitic magma being generated in the Gangdese arc at this same time.

## Acknowledgements

The authors acknowledge U.S. National Science Foundation grant EAR 1111586 from the Continental Dynamics Program, which supported a multidisciplinary study of the southern Lhasa Block margin. Comments on an earlier version of this manuscript by J.B. Chapman resulted in much needed improvements.

## Appendix A. Supplementary data

Supplementary data to this article can be found online at https://doi.org/10.1016/j.gr.2019.03.011.

## References

Annen, C., Blundy, J.D., Sparks, R.S.J., 2006a. The Genesis of intermediate and silicic magmas in deep crustal hot zones. J. Petrol. 47, 505–539.

Allégre, C.J., Courtillot, V., Tapponnier, P., Hirn, A., Mattauer, M., Coulon, C., Jaeger, J.J., Achache, J., Schärer, U., Marcoux, J., Burg, J.P., Girardeau, J., Armijo, R., Gariépy, C., Göpel, C., Tindong, L., Xuchang, X., Chenfa, C., Guangqin, L., Baoyu, L., Jiwen, T., Naiwen, W., Guoming, C., Tonglin, H., Xibin, W., Wanming, D., Huaibin, S., Yougong, C., Ji, Z., Hongrong, Q., Peisheng, B., Songchan, W., Bixiang, W., Yaoxiu, Z., Xu, R., 1984. Structure and evolution of the Himalayan-Tibet orogenic belt. Nature 307, 17–22.

Annen, C., Blundy, J.D., Sparks, R.S.J., 2006b. The Genesis of Intermediate and Silicic Magmas in Deep Crustal Hot zones. J. Petrol. 47, 505–539.

Beck, S.L., Zandt, G., Myers, S.C., Wallace, T.C., Silver, P.G., Drake, L., 1996. Crustal-thickness variations in the Central Andes. Geology 24, 407–410.

Bennett, V.C. and D.J. DePaolo,1987, Proterozoic crustal history of the western United States as determined by Neodymium isotopic mapping: Geol. Soc. Am. Bull. 99, 674–685.

Bird, P., 1978, Initiation of intracontinental subduction in the Himalaya. Jour. Geophys. Res. 83, 4975–4987.

Borg, S.G., D.J. DePaolo and B.M. Smith,1990, Isotopic structure and tectonics of the Central Transantarctic Mountains: J. Geophys. Res.: vol. 95, No. B5, 6647–67.

Cande, S.C., Patria, P., Dyment, J., 2010. Motion between the Indian, Antarctic and African plates in the early Cenozoic. Geophys. J. Int. 183, 127–149.

Chapman, J.B., Kapp, P., 2017. Tibetan magmatism database. Geochem. Geophys. Geosyst. 18, 4229–4234. https://doi.org/10.1002/2017GC007217.

Chapman, J. B., Ducea, M. N., Profeta, L. & DeCelles, P. G. Tracking changes in crustal thickness during orogenic evolution with Sr/Y; an example from the Western U.S. Cordillera. Geology 43, 919–923 (2015).

Chapman, J.B., Ducea1, M.N., Kapp, P., Gehrels, G.E., DeCelles, P.G., 2017. Spatial and temporal radiogenic isotopic trends of magmatism in Cordilleran orogens. Gondwana Res. 48, 189–204.

Chen, W., 2017. Determination of crustal thickness under Tibet from gravity-gradient data. J. Asian Earth Sci. 143, 315–325.

Chen, C.-H, DePaolo, D.J., Lan, C.-Y., 1996. Rb-Sr microchrons in the Manaslu Granite: Implications for Himalayan thermochronology: Earth Planet. Sci. Lett. 143, 125–135.

Clark, M.K., House, M. a., Royden, L.H., Whipple, K., Burchfiel, B.C., Zhang, X., and Tang, W., 2005, Late Cenozoic uplift of southeastern Tibet: Geology, v. 33, no. 6, p. 525, doi: https://doi.org/10.1130/G21265.1.

Copeland, P., Harrison, T.M., Kidd, W.S.F., Ronghua, X., and Yuquan, Z.,1987, Rapid early Miocene acceleration of uplift in the Gandese Belt, Xizang-southern Tibet, and its bearing on accommodation mechanisms of the India-Asia collision. Earth Planet. Sci. Lett. 86, 240–252.

Coulon, C., Maluski, H., Bollinger, C., Wang, S., 1986. Mesozoic and Cenozoic volcanic rocks from central and southern Tibet: 39Ar/40Ar dating, petrological characteristics and geodynamical significance. Earth Planet. Sci. Lett. 79, 281–302.

Currie, B.S., Rowley, D.B., Tabor, N.J., 2005. Middle Miocene paleoaltimetry of southern Tibet: Implications for the role of mantle thickening and delamination in the Himalayan orogen. Geology 33, 181–184.

Dai, J., Wang, C., Hourigan, J., Li, Z., Zhuang, G., 2013. Exhumation. History of the Gangdese Batholith, Southern Tibetan Plateau: Evidence from Apatite and Zircon (U-Th)/He Thermochronology: The Journal of Geology 121 (2), 155–172. https://doi.org/10.1086/669250.

Davidson J, De Silva S,2000, Composite volcanoes. In: Sigurdsson H (ed) Encyclopedia of volcanoes. Academic Press, London, pp 663–682.

Debon, F., Le Fort, P., Sheppard, S.M.F., and Sonet, J.,1986, The four plutonic belts of the Transhimalaya - Himalaya: a chemical, mineralogical, isotopic, and chronological synthesis along a Tibet - Nepal section. J. Petrol.21, 219–250.

DeCelles, P.G., Robinson, D.M., and Zandt, G.,2002, Implications of shortening in the Himalayan fold-thrust belt for uplift of the Tibetan Plateau. Tectonics 21, 1062.doi:https://doi.org/10.1029/2001TC001322.

DeCelles, P.G., Kapp, P., Gehrels, G.E., Ding, L., 2014. Paleocene-Eocene foreland basin evolution in the Himalaya of southern Tibet and Nepal: Implications for the age of initial India-Asia collision. Tectonics 33 (5), 824–849.

Deniel, C., Vidal, P., Fernandez, A., Le Fort, P., Peucat, J.-J., 1987. Isotopic study of the Manaslu granite (Himalaya, Nepal): inferences on the age and source of Himalayan leucogranites. Contrib. Mineral. Petrol. 96, 78–92.

DePaolo, D.J., 1981, A neodymium and strontium isotopic study of the Mesozoic calc-alkaline granitic batholiths of the Sierra Nevada and Peninsular Ranges, California: J. Geophys. Res. 86, 10470–10488.

DePaolo, D.J., 1985. Isotopic studies of processes in mafic magma chambers. I. the Kiglapait intrusion, Labrador: J. Petrology 26, 925–951.

DePaolo, D.J., Perry, F., and Baldridge, W.S.,1992, Crustal versus mantle sources of granitic magmas: a two-parameter model based on Nd isotopic studies. Earth Sci. Trans. Royal Soc. Edinburgh 83, 439–446.

Dewey, J.F., Shackelton, R.M., Chang Chengfa, and Sun Yiyin, 1988, The tectonic evolution of the Tibetan plateau. Phil. Trans. R. soc. Lond.A327, 379–413.

Ding, H., Zhang, Z., Dong, X., Tian, Z., Xiang, H., Mu, H., Gou, Z., Shui, X., Li, W., Mao, L., 2016. Early Eocene (c. 50 Ma) collision of the Indian and Asian continents: Constraints from the North Himalayan metamorphic rocks, southeastern Tibet. Earth Planet. Sci. Lett. 435, 64–73.

Ding, L., Xu, Q., Yue, Y., Wang, H., Cai, F., Li, S., 2014. The Andean-type Gangdese Mountains: paleoelevation record from the Paleocene–Eocene Linzhou Basin. Earth Planet. Sci. Lett. 392, 250–264.

Farmer, G.L. and D.J. DePaolo,1983, Origin of Mesozoic and Tertiary Granite in the Western U. S. and Implications for Pre-Mesozoic Crustal Structure. 1. Nd and Sr Isotopic Studies in the Geocline of the Northern Great Basin: J. Geophys. Res. 88, 3379–3401.

Farner, M.J., Lee, C.-T., 2017. Effects of crustal thickness on magmatic differentiation in subduction zone volcanism: a global study. Earth Planet. Sci. Lett. 470, 96–107.

Fromm, R., Zandt, G., Beck, S.L., 2004. Crustal thickness beneath the Andes and Sierras Pampeanas at 30°S inferred from Pn apparent phase velocities. Geophys. Res. Lett. v. 31. https://doi.org/10.1029/2003GL019231.

Gao, Z.F., Wilson, M., and Liu, J.Q.,2007, Post-collisional adakites in south Tibet: Products of partial melting of subduction-modified lower crust. Lithos 96, 205–224.

Gehrels, G., Rusmore, M., Woodsworth, G., Crawford, M., Andronicos, C., Hollister, L., Patchett, J., Ducea, M., Butler, R., Klepeis, K., Davidson, C., Friedman, R., Haggart, J., Mahoney, B., Crawford, W., Pearson, D., Girardi, J., 2009. U-Th-Pb geochronology of the Coast Mountains batholith in North-Coastal British Columbia: Constraints on age and tectonic evolution. Gelogical Society of America Bulletin 121, 1341–1361.

Guan, Q., Zhu, D.-C., Zhao, Z., Dong, G.-C., Zhang, L.-L., Li, X.-W., Liu, M., Mo, X.-X., Liu, Y.-S., Yuan, H.-L., 2012. Crustal thickening prior to 38 Ma in southern Tibet: evidence from lower crust-derived adakitic magmatism in the Gangdese Batholith. Gondwana Res. 21, 88–99.

Guillot, S., Hodges, K., LeFort, P., Pecher, A., 1994. New constraints on the age of the Manaslu granite - evidence for episodic tectonic denudation in the central Himalayas. Geology 22, 559–562.

Guillot, S., Mahéo, G., de Sigoyer, J., Hattori, K.H., Pêcher, A., 2008. Tethyan and Indian subduction viewed from the Himalayan high- to ultrahigh-pressure metamorphic rocks. Tectonophysics 451, 225–241.

Hammersley, L., and DePaolo, D.J.,2006, Isotopic and geophysical constraints on the structure and evolution of the Clear Lake volcanic system Jour. Volcan.Geotherm. Res. 153, 331–356.

Harris, N.B.W., Xu, R., Lewis, C.L., Hawkesworth, C.J., and Zhang, Y.,1988, Isotope geochemistry of the 1985 Tibet geotraverse, Lhasa to Golmud. Phil. Trans. Roy. Soc. Lond. A 327, 263–285.

Harrison, T.M., Copeland, P., Kidd, W.S.F., Yin, A., 1992. Raising Tibet. Science 255, 1663–1670.

Harrison, T.M., McKeegan, K.D., Le Fort, P., 1995. Detection of inherited monazite in the Manaslu leucogranite by 208Pb/232Th ion microprobe dating: crystallization age and tectonic significance. Earth Planet. Sci. Lett. 133, 271–282.

He, S.D., Kapp, P., DeCelles, P.G., Gehrels, G.E., and Heizler, M.,2007, Cretaceous-Tertiary geology of the Gangdese Arc in the Linzhou area, southern Tibet.Tectonophysics 433, 15–37.

Hildreth, W., 1981. Gradients in silicic magma chambers: Implications for lithospheric magmatism. J. Geophysical research 86, 10153–10192.

Hildreth, W., Moorbath, S., 1988. Crustal contributions to arc magmatism in the Andes of Central Chile. Contrib. Mineral. Petrol. 98, 455–489.

Hou, Z.Q., Gao, Y.F., Qu, X.M., Rui, Z.Y., Mo, X.X.,2004, Origin of adakiticintrusives generated during mid-Miocene east-west extension in southern Tibet. Earth Planet. Sci. Lett. 220, 139–155.

Hu, F., Ducea, M.N., Liu, S., Chapman, J.B., 2017. Quantifying Crustal Thickness in Continental Collisional Belts: Global Perspective and a. Geologic Application. Nature Scientific Reports v. 7. https://doi.org/10.1038/s41598-017-07849-7.

Hu, X., Garzanti, E., Moore, T., Raffi, I., 2015. Direct stratigraphic dating of India-Asia collision onset at the Selandian (middle Paleocene, 59±1 Ma). Geology 43 (10), 859–862.

Ingalls, M., Rowley, D.B., Olack, G., Currie, B.S., Li, S., Schmidt, J., Tremblay, M., Polissar, P.J., Shuster, D.L., Lin, D., Colman, A.S., 2017. Paleocene to Pliocene low-latitude high elevation of southern Tibet: Implications for tectonic models of India-Asia collision, Cenozoic climate, and geochemical weathering. Geological Society of America Bulletin v. 129. https://doi.org/10.1130/B31723.

Jellinek, A.M. and DePaolo, D.J.,2003, A model for the origin of large silicic magma chambers: precursors to caldera-forming eruptions. Bull. Volcanology 65, 363–381.

Ji, W.-Q., Wu, F.-Y., Liu, C.-Z., and Chung, S.-L.,2011, Early Eocene crustal thickening in southern Tibet: New age and geochemical constraints from the Gangdese batholith. Journal of Asian Earth Sciences, 53, 82–95.

Kang, Zhi-Qiang, Xu, Ji-Feng, Wilde, Simon A., Feng, Zuo-Hai, Chen, Jian-Lin, Bao-DiWang, Wen-Chun Fu, Pan, Hui-Bin, 2014. Geochronology and geochemistry of the Sangri Group Volcanic Rocks, Southern Lhasa Terrane: Implications for the early subduction history of the Neo-Tethys and Gangdese Magmatic Arc. Lithos 200-201, 157–168.

Kapp, J.L.D., Harrison, T.M., Kapp, P.A., Grove, M., Lovera, O.M. and Lin, D.,2005, The Nyainqentanglha Shan: A window into the tectonic, thermal and geochemical evolution of the Lhasa block, southern Tibet. Jour. Geophys. Res. 110, doi:https://doi.org/10.1029/2004JB003330.

Kay, S.M., Coira, B.L., Caffe, P.J., Chen, C.-H., 2010. Regional chemical diversity, crustal and mantle sources and evolution of central Andean Puna plateau ignimbrites. J. Volcanol. Geotherm. Res. 198, 81–111.

Kidd, W.S.F., Pan, Yusheng, Chang, Chenfa, Coward, M.P., Dewey, J.F., Gansser, A., Molnar, P., Shackleton, R.M., Yiyin, Sun, 1988. Geological mapping of the 1985 Chinese-British Tibetan (Xizang-Qinghai) Plateau geotraverse route. *Phil. Trans. Roy. Soc. London*. A 327, 287–305.

Laske, G., G. Masters, Z. Ma, and M. E. Pasyanos (2012), CRUST1.0: An updated global model of the Earth's crust, EGU General Assembly, 14, p. 3743. [http://igppweb.ucsd.edu/~gabi/crust1.html.]

Lee, Hao-Yang, Chung, Sun-Lin, Ji, Jianqing, Qian, Qing, Gallet, Sylvain, Lo, Ching-Hua, Lee, Tung-Yi, Zhang, Qi, 2012. Geochemical and Sr–Nd isotopic constraints on the genesis of the Cenozoic Linzizong volcanic successions, southern Tibet. J. Asian Earth Sci. 53, 96–114.

Leech, M.L., Singhb, T.S., Jainb, A.K., Klempererc, Simon L., Manickavasagam, R.M., 2005. The onset of India–Asia continental collision: early, steep subduction required by the timing of UHP metamorphism in the western Himalaya. Earth Planet. Sci. Lett. 234, 83–97.

Leeder, M.R., Smith, A.B., Yin, J., 1988. Sedimentology, palaeoecology and palaeoenvironmental evolution of the 1985 Lhasa to Golmud Geotraverse. Phil. Trans. R. Soc. Lond. A327, 107–143.

Mamani, M., Tassara, A., Wörner, G., 2008. Composition and structural control of crustal domains in the Central Andes: Geochemistry. Geophysics, Geosystems, v. 9. https://doi.org/10.1029/2007GC001925.

Mamani, M., Worner, G., Sempere, T., 2010. Geochemical variations in igneous rocks of the Central Andean orocline (13°S to 18°S): Tracing crustal thickening and magma generation through time and space. GSA Bull. 122, 162–182.

McGlashan, N., Brown, L., Kay, S., 2008. Crustal thickness in the Central Andes from teleseismically recorded depth phase precursors. Geophys. J. Int. 175, 1013–1022.

Mo, X.X., Hou, Z.Q., Niu, Y.L., Dong, G.C., Qu, X.M., Zhao, Z.D., and Yang, Z.M.,2007, Mantle contributions to crustal thickening during continental collision: evidence from Cenozoic igneous rocks in southern Tibet. Lithos 96, 225–242.

Molnar, P., 2005, Mio-Pliocene growth of the Tibetan Plateau and evolution of east Asian climate. Palaeontologia Electronica 8, 23p.

Molnar, P., England, P., and Martinod, J.,1993, Mantle dynamics, uplift of the Tibetan Plateau, and the Indian monsoon. Rev. Geophys. 31, 357–396.

Nabelek, J. et al.,2009, Underplating in the Himalaya-Tibet Collision Zone Revealed by the Hi-CLIMB Experiment. Science 325, 1371–1374.

Nomade, S., Renne, P.R., Mo, X., Zhao, Z., Zhou, S., 2004. Miocene volcanism in the Lhasa block, Tibet:spatial trends and geodynamic implications. Earth Planet. Sci. Lett. 221, 227–243.

Pasyanos, M.E., Masters, T.G., Laske, G., Ma, Z., 2014. LITHO1.0: An updated crust and lithospheric model of the Earth. J. Geophys. Res. Solid Earth 119, 2153–2173. https://doi.org/10.1002/2013JB010626.

Perry, F.V., D.J. DePaolo, and W.S. Baldridge,1993, Neodymium isotopic evidence for decreasing crustal contributions to Cenozoic ignimbrites of the western United States: Implications for the thermal evolution of the Cordilleran crust: Geol. Soc. Am. Bull, v. 105, p. 872–882.

Profeta, L., Ducea, M.N., Chapman, J.B., Paterson, S.R., Gonzalez, S.M.H., Kirsch, M., Petrescu, L., DeCelles, P.G., Quantifying crustal thickness over time in magmatic arcs: Sci. Rep. 5, doi:https://doi.org/10.1038/srep17786 (2015).

Reymer A, Schubert G,1984, Phanerozoic addition rates to the continental crust and crustal growth. Tectonics v.3, 63–77.

Schmidt, J.L., Tremblay, M.M., Wielicki, M.M., Zeitler, P.K., Schuster, D.L., 2019, Spatially variable Miocene denudation in southern and southeastern Tibet. (in preparation).

Tapponnier, P., Xu, Z.Q., Roger, F., Meyer, B., Arnaud, N., Wittlinger, G., and Yang, J.S.,2001, Geology: Oblique stepwise rise and growth of the Tibet plateau. Science 294, 1671-1677.

Tenzer, R., Chen, W., 2014. Regional gravity inversion of crustal thickness beneath the Tibetan plateau. Earth Sci. Inf. 7 (4), 265–276.

Tremblay, M.M., Fox, M., Schmidt, J.L., Tripthy-Lang, Wielicki, M.M., Harrison, T.M., Zeitler, P.K., Shuster, D.L., 2015. Erosion in southern Tibet shut down at ~10 Ma due to enhanced rock uplift within the Himalaya. Proc. Natl. Acad. Sci. 112, 12031–12035.

Wang, C., Dai, J., Zhao, X., Graham, S.A., He, D., Ran, B., Meng, J., 2014. Outward-growth of the Tibetan Plateau during the Cenozoic: a review. Tectonophysics 621, 1–43.

Xu, R.H., Scharer, U., Allegre, C.J., 1985. Magmatism and metamorphism in the Lhasa block (Tibet): a geochronological study. J.Geol. 93, 41–57.

Xu, Z.J., Song, X., Zhu, L., 2013. Crustal and uppermost mantle S velocity structure under Hi-CLIMB seismic array in central Tibetan Plateau from joint inversion of surface wave dispersion and receiver function data. Tectonophysics 584, 209–220.

Yin, A., Harrison, T.M., 2000. Geologic evolution of the Himalayan-Tibetan Orogen. Ann. Revs. Earth Planet. Sci. Lett. 28, 211–280.

Zhang, H., Harris, N., Parrish, R., Kelley, S., Zhang, L., Rogers, N., Argles, T., King, K., 2004. Causes and consequences of protracted melting of the mid-crust exposed in the North Himalayan antiform. Earth Planet. Sci. Lett. 228, 195–212.

Zhao, Z., Mo, X., Dilek, Y., Nu, Y., DePaolo, D.J., Robinson, P., Zhu, D-C., Sun, C., Dong, G., Luo, Z., Hou, Z., 2009. Geochemical and Sr–Nd–Pb–O isotopic compositions of the post-collisional ultrapotassic magmatism in SW Tibet: petrogenesis and implications for India intra-continental subduction beneath southern Tibet. Lithos 113, 190–212.

Zhu, D.C., Pan, G.T., Wang, L.Q., Mo, X.X., Zhao, Z.D., Zhou, C.Y., Liao, Z.L., Dong, G.C., Yuan, S.H., 2008. Spatio-temporal distribution and tectonic setting of Jurassic magmatism in the Gangdese belt, Tibet, China. Geological Bullletin of China 27, 458–468.

Zhu, D.-C., Zhao, Z-D., Niu, Y., Mo, X.-X., Chung, S.-L., Hou, Z.-Q.,2011, The Lhasa Terrane: Record of a microcontinent and its histories of drift and growth. Earth and Planetary Science Letters v. 301, p. 241–255.

Zhu, D.-C., Wang, Q., Cawood, P.A., Zhao, Z.-D., Mo, X.-X., 2017. Raising the Gangdese Mountains in southern Tibet. J. Geophys. Res-Sol. Ea. 122, 214–222.

View publication stats